Understanding the Chemical Dynamics of the Reactions of Dicarbon with 1-Butyne, 2-Butyne, and 1,2-Butadiene – Toward the Formation of Resonantly Stabilized Free Radicals†

Dorian S. N. Parker, S. Maity, Beni B. Dangi, Ralf I. Kaiser*

Department of Chemistry, University of Hawai'i at Manoa, Honolulu, HI 96822

Alexander Landera, A. M. Mebel*

Department of Chemistry & Biochemistry, Florida International University, Miami, FL 33199

† Electronic Supplementary Information (ESI) available: RRKM calculated rate constants for individual reaction steps of the $C_2(a^3\Pi_u/ X^1\Sigma_g^+)$ + C_4H_6 reactions (Table S1).

Abstract

The reaction dynamics of the dicarbon radical $C_2(a^3\Pi_u/ X^1\Sigma_g^+)$ in the singlet and triplet state with C_4H_6 isomers 2-butyne, 1-butyne and 1,2-butadiene were investigated at collision energies of about 26 kJ mol^{-1} using the crossed molecular beam technique and supported by *ab initio* and RRKM calculations. The reactions are all indirect, forming C_6H_6 complexes through barrierless additions by dicarbon on the triplet and singlet surfaces. Isomerization of the C_6H_6 reaction intermediate leads to product formation by hydrogen loss in a dicarbon-hydrogen atom exchange mechanism forming acyclic C_6H_5 reaction products through loose exit transition states in overall exoergic reactions.

1. Introduction

Complex carbon-based organic chemistry involving small unsaturated hydrocarbons and their radicals in the gas phase as seen in combustion environments and in the interstellar medium share the tendency toward mass growth culminating in the formation of polycyclic aromatic hydrocarbons (PAHs) and their (de)hydrogenated, alkyl-substituted, and ionized counterparts.[1-3] Despite the vast differences in these environments and the inherent lack of available molecular oxygen in the interstellar medium such as cold molecular clouds - the former typified by high pressures (5,000-46,000 Torr) and temperatures (900-2,000 K) while the latter by low pressures equivalent to about 10^{-14} Torr and temperatures as low as 10 K - the overall tendency toward mass growth and formation of PAHs and even carbonaceous nano structures is evident.[1, 3, 4] Both interstellar and terrestrial systems are under constant investigation by, for instance, the combustion chemistry community because we aim to eliminate incomplete combustion, reduce soot formation, and obtain the maximum energy release from fossil and bio fuels, while in the interstellar medium (ISM)[3, 5, 6] it is the chemistry of carbon that dominates the astrochemistry in particular in molecular clouds (TMC-1),[7] star forming regions (SgrB2),[8] circumstellar envelopes of dying carbon stars (IRC+10216),[9] and pre-planetary nebula[2] eventually linking the formation of PAHs to the origins of life.[10] The mass growth process starts at the molecular level and reaches particulate size of a few tens of nanometers initialized by reactions involving small unsaturated hydrocarbons C_xH_y (x=2-6, y=1-6) and resonantly stabilized free radicals (RSFRs).[11-14] Resonantly stabilized hydrocarbon radicals - radicals in which the unpaired electron is delocalized over the molecule – create thermodynamically stable and hence abundant molecules in combustion systems.[15] RSFRs are consequently found in high concentrations in extreme environments such as combustion flames and the interstellar medium.[16] Perhaps the best known example of an RSFR is the propargyl radical (H_2CCCH, X^2B_2), which has received considerable attention in its role in PAH formation particularly in forming the first cyclic structure, benzene (C_6H_6) and/or phenyl radicals (C_6H_5) via self-reaction.[17-19] Combustion flames have been found to contain C_4H_6 species such as 1,3-butadiene ($C_2H_3C_2H_3$), 2-butyne (CH_3CCCH_3), 1-butyne ($HCCC_2H_5$), and 1,2-butadiene ($H_2CCCH(CH_3)$), as well as dicarbon species.[11-13, 20] Based on our knowledge of reactions of dicarbon with unsaturated hydrocarbons as studied under single collision conditions exploiting the crossed molecular beams methods,[21] the reactions between

dicarbon and C_4H_6 isomers are predicted to be fast within gas kinetics limits (10^{-10} cm^3s^{-1}) and lead to the formation of resonantly and possibly aromatic radicals of the molecular formula C_6H_5 via the dicarbon versus atomic hydrogen exchange pathways that participate in the mass growth process.[22] Aromatic molecules such as the phenyl radical (C_6H_5) and benzene (C_6H_6) have been formed via reactions of dicarbon (C_2)[22] and the ethynyl radical (C_2H)[23] with 1,3-butadiene ($C_2H_3C_2H_3$); o-benzyne (C_6H_4) was synthesized via the reaction of the ethynyl radical (C_2H) with vinylacetylene (C_2H_3CCH);[24] these processes have been postulated to nucleate growth of PAHs by providing the sites onto which acyclic molecules and aromatic molecules bind and further cyclize.[1,25] Aromatization thermodynamically drives the reaction network and successive ring formation by RSFRs leads to large PAHs and eventually soot.[26, 27]

To aid the understanding of complex carbon mass growth processes, the underlying elementary bimolecular reactions have to be individually investigated to elucidate isomer specific sources of distinct RSFRs.[28] This can be conducted under single collision conditions exploiting cross molecular beam experiments.[29] Recall that the aromatic benzene,[30] the phenyl radical,[22] and o-benzyne[24] species can be formed via reactions of dicarbon and ethynyl radicals with 1,3-butadiene and vinylacetylene. On the other hand, the reactions of atomic carbon and dicarbon with unsaturated hydrocarbons ethylene (C_2H_4), methylacetylene (CH_3CCH), allene (H_2CCCH_2), propylene (C_3H_6), and vinylacetylene (C_2H_3CCH) form acyclic RSFRs: C_3H_3,[31] n-C_4H_3,[32-34] C_5H_3,[35-37] C_4H_5,[38, 39] and C_6H_3[40] (Table 1). It should be noted that in combustion systems, the C_4H_6 isomers are interconvertible either via thermally induced[41, 42] or atomic hydrogen assisted isomerization processes[43] involving relatively low energy barriers of only 15 kJ mol^{-1}. Interestingly, most combustion experiments probing flame components often only identify 1,3-butadiene[11-13] and occasionally 1,2-butadiene,[44] while leaving 1-butyne and 2-butyne unaccounted for, except for a recent investigation by Pousse et al., who successfully identified all four C_4H_6 isomers.[20] The lack of C_4H_6 isomer consideration has been commented on previously.[45] The commenter in Bakali et al.'s paper implies that omission of distinct isomers from flame models underrepresents the pool of reactive species. To account for this lack of data, we decided to investigate the reactions of the remaining C_4H_6 isomers, 2-butyne, 1-butyne, and 1,2-butadiene, with dicarbon (C_2; $a^3\Pi_u$/ $X^1\Sigma_g^+$) in an attempt to elucidate the formation of various C_6H_5 RSFRs formed together with their isomer-specific reaction mechanisms.

Table 1: Compilation of the formation of resonant stabilized free radicals (RSFRs) in the bimolecular reactions of atomic carbon $C(^3P_j)$ and dicarbon $C_2(a^3\Pi_u/X^1\Sigma_g^+)$ with unsaturated hydrocarbons ethylene (C_2H_4), methylacetylene (C_3H_4), allene (C_3H_4), propylene (C_3H_6), and vinylacetylene (C_4H_4).

	C_2H_4	C_3H_4		C_3H_6	C_4H_4
	Ethylene H_2CCH_2	Methyl-acetylene CH_3CCH	Allene H_2CCCH_2	Propylene C_3H_6	Vinylacetylene C_2H_3CCH
$C(^3P_j)$	C_3H_3 propargyl H_2CCCH 31 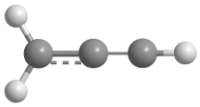	i-C_4H_3 1-buten-3-yn-2-yl H_2CCCCH 33, 34 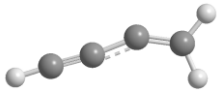		C_4H_5 1-methylpropargyl $H_3CHCCCH$ 38, 39 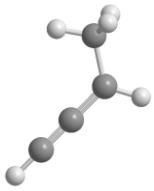 3-methylpropargyl H_2CCCCH_3 38, 39 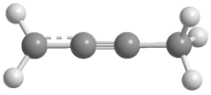	i-C_5H_3 2,4-pentadiiynyl-1 $H_2CCCCCH$ 37 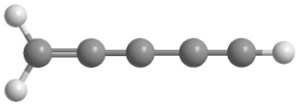 n-C_5H_3 1,4-pentadiynyl-3 HCCCHCH 37 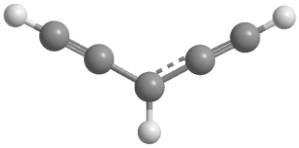
C_2 $(a^3\Pi_u/$ $X^1\Sigma_g^+)$	n-C_4H_3 1-buten-3-yn-2-yl H_2CCCCH 32 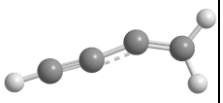	i-C_5H_3 2,4-pentadiiynyl-1 $H_2CCCCCH$ 35, 36 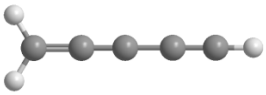 n-C_5H_3 1,4-pentadiynyl-3 HCCCHCH 36 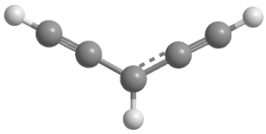		C_6H_3 1-hexene-3,4-diynyl-2 $H_2CCCCCCH$ 40 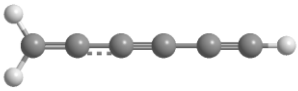

2. Experimental

The experiments were carried out under single collision conditions in a crossed molecular beams machine at the University of Hawaii.[21] A supersonic beam of dicarbon [$C_2(X^1\Sigma_g^+/a^3\Pi_u)$] in

both the ground and excited states [46] was produced by expanding a pulsed beam of neon (Ne, 99.9999%, Specialty Gases of America) within a laser ablation zone containing a rotating carbon rod in the primary source region of the vacuum chamber.[47] The carbon was ablated by focusing the 266 nm output of a Nd:YAG laser at energies of 10-15 mJ per pulse and operating at 30 Hz onto the graphite rod. The neon carrier gas with a backing pressure of 4 atm was introduced to the primary source via a Proch-Trickl pulsed valve, operating at 60 Hz with amplitudes of -400 V and opening times of 80 μs. During the ablation of the graphite rod, both atomic carbon and tricarbon are produced in sizeable quantities as well as dicarbon. The reaction products of atomic carbon with all C_4H_6 isomers have a lower mass of 65 amu than those of the dicarbon - C_4H_6 reaction products.[48-50, 62] Previous studies of reactions of tricarbon molecules with unsaturated hydrocarbons like allene, methylacetylene, acetylene, and ethylene showed the existence of entrance barriers of at least 45 kJ mol^{-1},[51,61] which are higher than our collision energies. Therefore, neither ground-state carbon atoms nor tricarbon molecules interfered with the reactive scattering signal to probe the formation of C_6H_5 isomers. The dicarbon molecular beam passed a skimmer and a four-slot chopper wheel, which selected a segment of the pulsed beam with a well-defined peak velocity (v_p) and speed ratio (S). The primary beam characteristics were v_p = 1758 ± 20 ms^{-1} and S = 2.7 ± 0.1 (Table 2). The dicarbon beam subsequently crosses perpendicularly at a pulsed beam of the secondary reactant [1-butyne, 98.0%, Aldrich), 2-butyne (99.0%, Aldrich), or 1,2-butadiene (99.0%, Aldrich) released by a second pulsed valve at 550 Torr with peak velocities of v_p = 790 ± 10, 800 ± 10, and 790 ± 10 ms^{-1} and speed ratio of 6.1 ± 0.2, 5.8 ± 0.2 and 8.0 ± 0.2, respectively (Table 2). The secondary pulsed valve was operated at repetition rates of 60 Hz, amplitudes of -450 V and opening times of 80 μs. The primary pulsed valve opened 15 μs after the secondary pulsed valve and 1880 μs after time zero as defined by the chopper wheel. The resultant collision energy between the dicarbon and the secondary beams, 1-butyne, 2-butyne, and 1,2-butadiene were 26.4 ± 0.6, 25.5 ± 0.6, and 24.9 ± 0.6 kJ mol^{-1}, respectively.

The dicarbon molecular beam generated by laser ablation produces molecules in both their singlet ground ($X^1\Sigma_g^+$) and first excited ($a^3\Pi_u$) electronic states. To understand the contributions made by different electronic states to the reaction dynamics the ro-vibrational distributions were characterized *in situ* by laser induced fluorescence spectroscopy.[21, 22] Table 3 summarizes the

distributions of rotational temperatures (T_{rot}) and populations of vibrational levels observed (v=0 and v=1) in the singlet and triplet states through probing the Muliken excitation ($D^1\Sigma_u^+$- $X^1\Sigma_g^+$) and the Swan system ($d^3\Pi_g$ - $a^3\Pi_u$), respectively.

Table 2: Peak velocities (v_p), speed ratio (S), and the center-of-mass angles (Θ_{CM}), together with the nominal collision energies (E_{col}) of ethylene and boron oxide molecular beams.

	v_p(ms^{-1})	S	E_{col} (kJ mol^{-1})	Θ_{CM}
CH_3CCCH_3 (X^1A_{1g})	800 ± 10	5.8 ± 0.2	26.4 ± 0.6	47.1 ± 1.0
CH_3CH_2CCH (X^1A')	790 ± 10	6.1 ± 0.2	25.5 ± 0.6	47.7 ± 1.0
CH_3CHCCH_2 (X^1A')	790 ± 10	8.0 ± 0.2	24.9 ± 0.6	48.5 ± 1.0
C_2 ($X^1\Sigma_g^+/a^3\Pi_u$)	1758 ± 20	2.6 ± 0.1		

Table 3: Vibrational and Rotational Energy Distribution in the Two Lowest Electronic States of Dicarbon.

Electronic State	Temp, K	v =0	v=1
Triplet ($a^3\Pi_u$)	Total	68%	32%
	50	45%	20%
	300	23%	12%
Singlet ($X^1\Sigma_g^+$)	Total	83%	17%
	200	44%	6%
	1,000	39%	11%

The reaction products were monitored using a triply differentially pumped quadrupole mass spectrometer (QMS) in the time-of-flight (TOF) mode after electron-impact ionization of the neutral molecules at 80 eV with an emission current of 2 mA. These charged particles were separated according to their mass-to-charge ratio by an Extrel QC 150 quadruple mass spectrometer (QMS) operated with an oscillator at 2.1 MHz; only ions with the desired mass-to-charge, m/z, value passed through and were accelerated toward a stainless steel 'door knob' target coated with an aluminum layer and operated at a voltage of -22.5 kV. The ions hit the surface and initiated an electron cascade that was accelerated by the same potential until they reached an aluminum coated organic scintillator whose photon cascade was detected by a photomultiplier tube (PMT, Burle, Model 8850, operated at -1.35 kV). TOF spectra were recorded at 2.5°

intervals over the angular distribution. The TOF spectra recorded at each angle and the product angular distribution in the laboratory frame (LAB) were fit with Legendre polynomials using a forward-convolution routine. This method uses an initial choice of the product translational energy $P(E_T)$ and the angular distribution $T(\theta)$ in the center-of-mass reference frame (CM) to generate the TOF spectra and a product angular distribution. The TOF spectra and product angular distribution obtained from the fit were then compared to the experimental data. The parameters $P(E_T)$ and $T(\theta)$ were iteratively optimized until the best fit was reached.

3. Theoretical Methods

Stationary points on the singlet and triplet C_6H_6 potential energy surfaces (PES) accessed by the reactions of $C_2(^1\Sigma_g^+/^3\Pi_u)$ with the C_4H_6 isomers, including intermediates, transition states, and possible products, were optimized at the hybrid density functional B3LYP level of theory[52,53] with the 6-311G** basis set. Vibrational frequencies were computed using the same B3LYP/6-311G** method and were used to obtain zero-point vibrational energy (ZPE) corrections. Relative energies of various species were refined employing the coupled cluster CCSD(T) method[54] with Dunning's correlation-consistent cc-pVDZ and cc-pVTZ basis sets.[55] Then the total energies were extrapolated to the complete basis set (CBS) limit using the equation $E_{total}(CBS) = (E_{total}(VTZ)-E_{total}(VDZ)\times 2.5^3/3.5^3)/(1-2.5^3/3.5^3)$.[56] Relative energies discussed in the paper are thus computed at the CCSD(T)/CBS(dt)//B3LYP/6-311G** + ZPE(B3LYP/6-311G**) level of theory with two-point CBS extrapolation and are expected to be accurate within $\pm$15 kJ mol^{-1}. For the key reaction products, we additionally performed CCSD(T)/cc-pVQZ calculations and the CCSD(T) total energies were extrapolated to the CBS limit by fitting the following equation, $E_{tot}(x) = E_{tot}(\infty) + Be^{-Cx}$, where x is the cardinal number of the basis set (2, 3, and 4 for cc-pVDZ. cc-pVTZ, and cc-pVQZ, respectively) and $E_{tot}(\infty)$ is the CCSD(T)/CBS(dtq) total energy. The CCSD(T)/CBS(dtq) reaction energies are normally accurate within $\pm$10 kJ mol^{-1}. The B3LYP and CCSD(T) quantum chemical calculations were performed using the GAUSSIAN 09[57] and MOLPRO 2010[58] program packages.

Unimolecular rate constants of all unimolecular reaction steps on the singlet and triplet PES following initial association of $C_2(^1\Sigma_g^+/^3\Pi_u)$ with 1-butyne, 2-butyne, and 1,2-butdiene were

computed using Rice-Ramsperger-Kassel-Marcus (RRKM) theory,[59] as functions of available internal energy of each intermediate or transition state. In RRKM theory, a rate constant $k(E)$ at an internal energy E for a unimolecular reaction $A^* \rightarrow A^{\#} \rightarrow P$ is expressed as

$$k(E) = \frac{\sigma}{h} * \frac{W^{\neq}(E - E^{\neq})}{\rho(E)},$$

where σ is the reaction path degeneracy, h is Plank's constant, $W^{\#}(E\text{-}E^{\#})$ denotes the total number of states for the transition state (activated complex) $A^{\#}$ with a barrier $E^{\#}$, $\rho(E)$ represents the density of states of the energized reactant molecule A*, and P is the product or products. In our calculations, the internal energy was taken as a sum of the collision energy and a negative of the relative energy of a species with respect to the reactants (the chemical activation energy). One energy level was considered throughout as at a zero pressure limit. Numbers and densities of states were obtained within the harmonic approximation using B3LYP/6-311G** computed frequencies. For H and CH_3 elimination channels on the singlet surface occurring without an exit barrier, rate constants were computed using microcanonical variational transition state theory (VTST).[59,60] In the microcanonical VTST, the minimum in the microcanonical rate constant is located along the reaction path according to the following equation:

$$\frac{dk(E)}{dq^{\#}} = 0,$$

where $q^{\#}$ is the reaction coordinate. To find the minimal value of $k(E)$ we first calculated a series of energies at different values of the reaction coordinate in question. To obtain these energies, we performed partial B3LYP/6-311G** geometry optimization with fixed values of the reaction coordinate and all other geometric parameters being optimized. Then, we calculated $3N$-7 vibrational frequencies projecting the reaction coordinate out. The B3LYP/6-311G** energies were multiplied by a scaling factor in order to match B3LYP/6-311G** and CCSD(T)/CBS(dt) energies of the final dissociation products, where the scaling factor was computed as the ratio of the relative energies of the products calculated at the CCSD(T)/CBS(dt) and B3LYP/6-311G** levels. All RRKM and VTST rate constants were utilized to compute product branching ratios by solving first-order kinetic equations within steady-state approximation:

$$\frac{d[C]_i}{dt} = \sum k_n [C]_j - \sum k_m [C]_i ,$$

where $[C]_i$ and $[C]_j$ are concentrations of various intermediates or products, k_n and k_m are microcanonical rate constants.

It should be noted that C_2 additions can occur barrierlessly to different double and triple bonds (unsaturated carbon atoms) in the C_4H_6 isomers. Evaluation of branching of the reaction flux in the entrance reaction channels, which proceed without barriers, often via the same kinetic bottleneck (a variational transition state) at large separations, is a dynamics problem. This problem can be in principle solved using ab initio calculations of quasiclassical trajectories in the entrance channels, but these time-consuming calculations are beyond the scope of the present study. Instead, here we address product branching ratios for various dissociation channels of chemically activated C_6H_6 adducts formed by C_2 additions to different sites of 2-butyne, 1-butyne, and 1,2-butadiene under single-collision conditions. As the calculations will show, the product branching ratios appear to be sensitive to the initial site of C_2 addition only for the reaction of triplet $C_2(^3\Pi_u)$ with 1,2-butadiene, but not sensitive for the other five reactions considered in this work.

4. Results

Reactive scattering signals for all three reactions were observed at m/z = 77 ($C_6H_5^+$) and m/z = 76 ($C_6H_4^+$). At each angle, the time-of-flight (TOF) spectra at m/z = 76 were, after scaling, identical to those at m/z = 77, indicating that signal at the lower *m*/*z* ratios originated for each system through dissociative electron impact ionization of the C_6H_5 parent molecules in the electron impact ionizer. Reactive scattering signal at m/z = 77 corresponds to the formation of a product with the molecular formula C_6H_5 and atomic hydrogen as a counter fragment. Therefore, we can conclude that the reaction of dicarbon with the C_4H_6 isomers 2-butyne (CH_3CCCH_3), 1-butyne (CH_3CH_2CCH), and 1,2-butadiene (CH_3CHCCH_3) are forming C_6H_5 products through atomic hydrogen loss. The reactive scattering signal for each system, 2-butyne (CH_3CCCH_3), 1-butyne (CH_3CH_2CCH) and 1,2-butadiene (CH_3CHCCH_3), is shown in Figures 1, 2 and 3 with laboratory angular distributions in the top left labeled (a), and selected time-of-flight (TOF)

profiles in the bottom left labeled (b) of each figure. Each system shows a broad laboratory angular distribution at m/z = 77 spread over at least 40° within the scattering plane. Further, all systems show their laboratory angular distribution peaking close to the center-of-mass angle. These results suggest that the reactions in each system proceeds via indirect scattering dynamics via C_6H_6 complex formation. The reactive signals from methyl (CH_3) loss reactions, which would yield (C_5H_3) products at m/z = 63, were searched for in all three reactions. However no reactive signals were observed. Signal contributions from the reaction of atomic carbon with the C_4H_6 isomers to form C_5H_5 plus atomic hydrogen (65 amu) that subsequently fragmented by electron impact ionization to C_5H_3 (63 amu) provided a significant background signal to observe any reactive signal from the methyl loss route in the reaction of dicarbon with the C_4H_6 isomers.

A forward convolution fitting routine was used to transform the laboratory data into the center-of-mass reference frame to help us gain information on the chemical dynamics of the systems. Best fits to laboratory data for all three systems were obtained with a single channel as shown by the red lines in Figures 1, 2, and 3. The center-of-mass translational energy distribution and angular distribution derived from the fit to the experimental data for 2-butyne (CH_3CCCH_3), 1-butyne (CH_3CH_2CCH), and 1,2-butadiene (CH_3CHCCH_3) are labeled (c) and (d) in Figures 1, 2 and 3, respectively. Based on the conservation of energy, we are able to calculate the reaction exoergicities by subtracting the collision energy of about 26 kJ mol^{-1} (Table 2) from the maximum translational energy released. For the reactions of dicarbon with 2-butyne, 1-butyne, and 1,2-butadiene, we find that the formation of the C_6H_5 isomer(s) plus atomic hydrogen is exoergic by a maximum of 218 ± 22 kJ mol^{-1}, 228 ± 31 kJ mol^{-1}, and 213 ± 28 kJ mol^{-1}, respectively. It should be considered that the enthalpy of formation of the triplet C_2 ($a^3\Pi_u$, $v = 0$) state is about 7.3 kJ mol^{-1} higher in energy than the singlet $C_2(X^1\Sigma_g^+)$ state when interpreting these reaction energies. Further, the $P(E_T)$s depict that the flux distributions peak away from zero translational energy. The dicarbon - 2-butyne reaction shows almost zero exit barrier of around 10 kJ mol^{-1}, while dicarbon - 1-butyne has a fairly large exit barrier of around 29 kJ mol^{-1} and the dicarbon - 1,2-butadiene system displays a similar magnitude exit barrier of 25 kJ mol^{-1}. These findings suggest that at least one reaction channel to form the C_6H_5 isomer(s) has a tight exit transition state and involves a repulsive carbon-hydrogen bond rupture with a significant electron rearrangement. Further, the data depict fractions of the average energy released into the

translational degrees of freedom of the products to be 23 %, 29 %, and 28 % of the total available energy. These orders of magnitude also propose indirect scattering dynamics. Finally, the center-of-mass angular distributions, T(θ), for all three systems are depicted in the bottom panels of Figures 1, 2, and 3; these distributions possess similar shapes and provide us with important information about the chemical dynamics. The distribution shows intensity over the whole angular range which is indicative of an indirect, complex-forming reaction mechanism involving C_6H_6 reaction intermediate(s). Secondly, the center-of-mass angular distributions are isotropic suggesting that the lifetime of the decomposing complex is longer than their rotational periods. The non-polarization or flatness of the T(θ) is indicative of poor coupling between the initial (L) and final (L') orbital angular momentum of the system. Typically, L is about 0.2 of L' for a reaction without an entrance barrier and within the orbiting limits.[63] The poor coupling is attributed to the lightness of the departing hydrogen atom that is not able to carry away enough angular momentum when emitted from the decomposing C_6H_6 complex. The C_6H_5 product formed carries away the majority of the total angular momentum of the system and is rotationally excited as a result.

5. Theoretical Results

The chemical dynamics of the reactions investigated here are best understood with an accurate description of the C_6H_6 potential energy surface for each system. The primary beam is composed of dicarbon radicals in their ground singlet state ($X^1\Sigma_g^+$) and in their first excited triplet state ($a^3\Pi_u$). This implies for each system we must analyze the singlet and triplet C_6H_6 potential energy surfaces (PES).

5.1 $C_2(X^1\Sigma_g^+/a^3\Pi_u)$ + 2-butyne (CH_3CCCH_3)

We are reporting now the results of a computational investigation of the reaction of singlet dicarbon ($C_2(X^1\Sigma_g^+)$) with 2-butyne (CH_3CCCH_3) as depicted by the schematic representation of the C_6H_6 PES in Fig. 4a. The calculations predict two feasible entrance channels involving the barrierless addition of dicarbon to both central carbon atoms of 2-butyne leading to a three-member carbon ring intermediate **i1$_{2b}$** or to a four-member ring structure **i2$_{2b}$**. Intermediate **i1$_{2b}$**

can isomerize to **i2$_{2b}$** and the latter subsequently isomerizes to the energetically more stable 2,4-hexadiyne isomer (**i3$_{2b}$**), which holds the lowest in energy minimum of this part of the singlet C_6H_6 PES. Intermediate **i3$_{2b}$** can emit a methyl group to form **p2$_{2b}$** (CH_3CCCC) or eject a hydrogen atom from either methyl group leading to **p1$_{2b}$** ($CH_3CCCCCH_2$); both decomposition pathways hold loose exit transition states as the single bond cleavage reactions feature no exit barriers.

The triplet $C_2(a^3\Pi_u)$ reaction with 2-butyne (Figure 4b) is initiated by addition to the triple C-C bond to produce a three-member ring intermediate **i4$_{2b}$** or to either of the central carbons forming intermediate **i5$_{2b}$**. Intermediate **i4$_{2b}$** can isomerize to **i5$_{2b}$** or alternatively rearrange to a bicyclic intermediate **i6$_{2b}$**. The structure of **i6$_{2b}$** features a rhombic C_4 core linked with two outside methyl groups. The rings in **i6$_{2b}$** can open in two consecutive steps to form a chain intermediate **i8$_{2b}$** through a three-member cyclic structure **i7$_{2b}$**. Intermediate **i8$_{2b}$** can lose a hydrogen atom from one of the CH_3 groups to form product **p1$_{2b}$**. In another reaction pathway, intermediate **i5$_{2b}$** can undergo a methyl emission to yield $CCCCCH_3$. **i5$_{2b}$** can also isomerize to **i9$_{2b}$** and **i10$_{2b}$**; these pathways are associated with 1,4- and 1,5-hydrogen migrations from the methyl groups to the former dicarbon unit. **i10$_{2b}$** can dissociate by losing hydrogen atoms from the CH_3 and CH_2 groups producing **p3$_{2b}$** ($H_2CCC(CH_2)CCH$) and **p4$_{2b}$** ($H_3CC(C_2H)_2$). Otherwise, from intermediate **i9$_{2b}$**, triplet carbene CH_2 emission yields **p5$_{2b}$** ($HCCCCCH_3$) and a hydrogen emission from the methyl group forms **p3$_{2b}$**.

5.2 $C_2(X^1\Sigma_g^+/a^3\Pi_u)$ + 1-butyne (CH_3CH_2CCH)

As shown in Figure 5a, the singlet C_2 ($X^1\Sigma_g^+$) plus 1-butyne reaction proceeds by barrierless addition of dicarbon to both acetyl carbons to yield a three-member ring intermediate **i1$_{1b}$** or a four-member ring structure **i2$_{1b}$**. Intermediate **i1$_{1b}$** rearranges to **i2$_{1b}$** and the latter further isomerizes to **i3$_{1b}$**, resulting in insertion of the C_2 unit into the acetyl chain. From intermediate **i3$_{1b}$**, three product channels are available through loose transition states: methyl emission yields **p2$_{1b}$** ($H_2CCCCCH$, *i*-C_5H_3), atomic hydrogen emission from the CH_2 group yields **p1$_{1b}$** ($H_3CCHCCCCH$), and H emission from the CH_3 group furnishes **p3$_{1b}$** (H_2CCH_2CCCCH).

The triplet C_2 + 1-butyne reaction shows C_2 addition to occur through three channels (Figure 5b); addition to the CH end group to yield **i8$_{1b}$**, to the bare central carbon atom of the acetyl group to yield **i5$_{1b}$**, or to the C≡C triple bond to form a three-member cyclic structure of intermediate **i4$_{1b}$**. Intermediate **i4$_{1b}$** can isomerize to either **i5$_{1b}$** or **i8$_{1b}$** by the three-member ring opening; **i5$_{1b}$** and **i8$_{1b}$** are also connected via a four-member cyclic intermediate **i6$_{1b}$**. From **i6$_{1b}$**, isomerization of the four-member cycle to a linear carbon chain yields intermediate **i7$_{1b}$**, which in turn can form products by emitting a hydrogen atom to yield **p1$_{1b}$** or a methyl group to reach product *i*-C_5H_3 **p2$_{1b}$**. The intermediate **i7$_{1b}$** alternatively can further isomerize by 1,3-hydrogen migration from the CH_3 group to the carbon chain over a small energy barrier to reach **i9$_{1b}$**. Intermediate **i9$_{1b}$** can undergo a hydrogen emission either from the CH group to yield **p3$_{1b}$** or from the central CH_2 group to yield **p4$_{1b}$** ($H_2CCHCCHCCH$). Further isomerization of **i9$_{1b}$** can occur, first through rotation to **i10$_{1b}$**, followed by bending of the acetyl group to reach **i11$_{1b}$**. Intermediate **i11$_{1b}$** is also accessible from **i8$_{1b}$** through hydrogen migration from the terminal CH_3 group to the terminal carbon on the opposite side. Intermediate **i11$_{1b}$** can cyclize to **i12$_{1b}$** and the latter subsequently re-distributes its hydrogen atoms from the CH_2 groups to the open carbon atoms of the cycle to first reach **i16$_{1b}$**, then **i17$_{1b}$**, and finally arriving at the benzene structure of triplet intermediate **i18$_{1b}$**. **i16$_{1b}$** and **i17$_{1b}$** can emit a hydrogen atom from the CH_2 groups through tight exit barriers to yield the phenyl radical product **p5$_{1b}$**. Intermediate **i18$_{1b}$** can also access the phenyl radical **p5$_{1b}$** through a loose exit transition state by emitting a hydrogen atom, or can isomerize to **i19$_{1b}$**, which can emit a CH group to reach the cyclopentadienyl radical **p6$_{1b}$** product through a loose transition state. Intermediate **i9$_{1b}$** can undergo hydrogen migration from the central CH_2 group to the neighboring carbon atom to reach **i13$_{1b}$**. Hydrogen emission from **i13$_{1b}$** from the CH group next to the CH_2 group yields the product **p7$_{1b}$** (*trans*-$H_2CCCHCHCCH$), whereas H losses from the neighboring CH groups give the products **p8$_{1b}$** ($H_2CCHCCHCCH$) and **p10$_{1b}$** ($H_2CCHCHCCCH$). Alternatively, rotation of the acetyl group in **i13$_{1b}$** leads to **i14$_{1b}$**, followed by further rotation to access **i15$_{1b}$**. Intermediate **i14$_{1b}$** can dissociate to the product **p9$_{1b}$** (*cis* conformation of $H_2CCCHCHCCH$) via the hydrogen emission from the second carbon. Finally, intermediate **i16$_{1b}$** can be reached by cyclization of **i15$_{1b}$**.

5.3 C_2 ($X^1\Sigma_g^+/a^3\Pi_u$) + 1,2-butadiene (CH_3CHCCH_3)

The singlet C_2 + 1,2-butadiene reaction as depicted in Figure 6a shows one open barrier-less entrance channel that occurs through addition of C_2 to the allyl group leading to a three-member cyclic structure of intermediate **i1$_{bd}$**. Intermediate **i1$_{bd}$** reaches intermediate **i2$_{bd}$** through insertion of the C_2 group into the carbon chain. Intermediate **i2$_{bd}$** can undergo methyl emission to yield **p2$_{bd}$** (*i*-C_5H_3; the same as **p2$_{1b)}$** or emit a hydrogen atom from the CH group to yield **p1$_{bd}$** ($H_3CCCCCCH_2$, the same as **p1$_{2b}$**), from the CH_2 group to yield **p3$_{bd}$** ($H_3CCHCCCCH$, the same as **p1$_{1b)}$**, or from the CH_3 group to yield **p4$_{bd}$** ($H_2CCHCCCCH_2$).

The triplet C_2 + 1,2-butadiene reaction shows C_2 to add in three separate locations all without entrance barriers, to the CH_2 group leading to **i6$_{bd}$**, to the CH group leading to **i9$_{bd}$** or to the bare carbon atom forming **i3$_{bd}$**. Intermediate **i9$_{bd}$** can undergo methyl emission to yield **p7$_{bd}$**. Furthermore, intermediate **i9$_{bd}$** can bind its C_2 group to form a four-member cyclic structure **i13$_{bd}$**. Opening of the four-member ring leads to **i17$_{bd}$** and hydrogen emission from the CH, CH_2, and CH_3 groups in this intermediate yields **p1$_{bd}$**, **p3$_{bd}$**, and **p4$_{bd}$**. The methyl group loss from **i17$_{bd}$** produces *i*-C_5H_3 **p2$_{bd}$**. Intermediate **i3$_{bd}$** can isomerize to **i6$_{bd}$** by forming a four-member cyclic intermediate **i5$_{bd}$**. Similarly, **i3$_{bd}$** can also rearrange to **i9$_{bd}$** via the four-member cyclic intermediate **i13$_{bd}$**. Intermediate **i6$_{bd}$** can access products **p5$_{bd}$** and **p6$_{bd}$** through methyl emission and hydrogen atom emission from the CH_2 group. Alternatively, **i6$_{bd}$** can isomerize by hydrogen migration from the CH_3 group to the terminal carbon atom to reach intermediate **i8$_{bd}$**. **i8$_{bd}$** can undergo atomic hydrogen emission from the CH group to reach the product **p8$_{bd}$**. Hydrogen emission from the central CH_2 group of **i8$_{bd}$** leads to product **p10$_{bd}$** (the same as **p4$_{1b}$**). Intermediate **i8$_{bd}$** can alternatively cyclize to reach intermediate **i11$_{bd}$**, which can isomerize through hydrogen migration from the CH_2 group to the neighboring bare carbon atom to reach **i12$_{bd}$** (**i16$_{1b}$**). The phenyl radical product (**p11$_{bd}$** = **p5$_{1b}$**) channel is accessible from **i12$_{bd}$** by hydrogen emission from the remaining CH_2 group. Further isomerization of **i12$_{bd}$** through hydrogen migration from the CH group to another CH group leads to **i15$_{bd}$**. The cyclic structure of **i15$_{bd}$** can be opened to reach **i16$_{bd}$**. Hydrogen emission from the central CH group of **i16$_{bd}$** accesses the product channel of **p4$_{bd}$**. The initial intermediate **i3$_{bd}$** can undergo hydrogen migration to the terminal bare carbon atom to reach **i4$_{bd}$**. Emission of a hydrogen atom from the central CH group accesses the product **p9$_{bd}$** ($H_2CCC(CH_2)CCH$). Intermediate **i4$_{bd}$** can also

cyclize to a five-member cyclic structure to reach **i7$_{bd}$**, which can isomerize to **i11$_{bd}$** in two steps, first forming a bicyclic structure **i10$_{bd}$** that opens to the six-member ring structure.

6. Discussion

The crossed beam experiments for the reactions of dicarbon with 2-butyne, 1-butyne and 1,2-butadiene share similar results that can help us elucidate the reaction dynamics in each system and will now be discussed. Firstly, each reaction proceeds through an atomic hydrogen – dicarbon exchange mechanism to form a molecule with the gross molecular formula, C_6H_5. No other product channels were found involving other mass-to-charge ratios. Secondly, the center-of-mass angular distributions show intensity over the full angular range and are isotropic indicating that each reaction proceeds by indirect scattering dynamics involving the formation of long lived collision complex(es) that undergo multiple isomerization steps before hydrogen atom emission. Thirdly, all three reactions are exothermic. Now we shall interpret the center-of-mass product translational energy distributions in each system to identify the products formed. By interpreting the center-of-mass product translation energy distribution with respect to the electronic structure calculations we can ascertain which isomer is being formed.

For the C_2 + 2-butyne system a reaction energy of 218 ± 22 kJ mol^{-1} was found. The reaction energy most closely matches the formation of product **p1$_{2b}$** plus atomic hydrogen on the singlet surface at -223 kJ mol^{-1} as shown in Figure 4 (a). Product **p1$_{2b}$** is the only C_6H_5 isomer able to be formed on the singlet surface and matches the reaction energy well. In this case addition of singlet dicarbon occurs to the acetyl bond creating a three-member ring intermediate **i1$_{2b}$** that isomerizes to a four-member ring intermediate **i2$_{2b}$** over a small barrier to reach the stable intermediate **i3$_{2b}$** 2,4-hexadiyne. 2,4-hexadiyne undergoes hydrogen emission from the methyl group through a loose transition state to reach **p1$_{2b}$**. The near zero peaking of P(E$_t$) is indicative of no exit barrier to product formation and is in line with formation of product **p1$_{2b}$** without an exit barrier on the singlet PES. On the triplet surface for the C_2 + 2-butyne system, RRKM calculations at the experimental collision energy show the formation of 44% of **p4$_{2b}$** via the **i5$_{2b}$** and **i10$_{2b}$** intermediates, 14.5% of **p1$_{2b}$** via the **i4$_{2b}$** → **i6$_{2b}$** → **i7$_{2b}$** → **i8$_{2b}$** pathway, and 41.5% of

p2$_{2b}$ produced by the methyl group loss from **i5$_{2b}$**; the results are independent on the relative abundances of the initial **i4$_{2b}$** and **i5$_{2b}$** intermediates. The experimental reaction energy matches the products **p4$_{2b}$** (at -228 kJ mol^{-1}) and **p1$_{2b}$** (at -234 kJ mol^{-1}), fitting theoretical predictions that they are the dominant C_6H_5 products formed.

In the C_2 + 1-butyne system, a reaction energy of 228 ± 31 kJ mol^{-1} was obtained which matches the formation energy of **p1$_{1b}$** plus atomic hydrogen at 230 kJ mol^{-1} on the singlet surface. The only other contending atomic hydrogen loss pathway is to **p3$_{1b}$** plus atomic hydrogen with a reaction energy of 166 kJ mol^{-1} which does not match our reaction energy. The reaction initiates by singlet dicarbon binding to both acetyl carbons to form three-member ring **i1$_{1b}$** or four-member ring **i2$_{1b}$** without entrance barriers; the two initial intermediates can easily rearrange into one another. Intermediate **i2$_{1b}$** further isomerizes to **i3$_{1b}$** by insertion of the C_2 unit in the carbon chain to form a diacetyl group. Subsequent atomic hydrogen emission from the CH_2 group in **i3$_{1b}$** produces **p1$_{1b}$** plus atomic hydrogen through a loose exit transition state in an overall exoergic reaction. The near-zero peaking of the product translational energy distribution indicates the absence of an exit barrier as seen on this reaction pathway. Formation of **p1$_{1b}$** is supported by RRKM theory calculations which predict 86% of the hydrogen loss products are **p1$_{1b}$** with the remaining being **p3$_{1b}$**. However, the calculations also predict that 92% of the total products undergo methyl loss to form *i*-C_5H_3 **p2$_{1b}$**. On the triplet surface there are six product channels leading to C_6H_5 isomers via atomic hydrogen loss that are within the acceptable range of energies within our error boundaries of ± 31 kJ mol^{-1} for experiment plus ± 10 kJ mol^{-1} for theory. Considering our reaction energy of 228 ± 31 kJ mol^{-1} products **p1$_{1b}$**, **p4$_{1b}$**, **p7$_{1b}$**, **p8$_{1b}$**, **p9$_{1b}$**, and **p10$_{1b}$** could be formed. It should be noted that products slightly below the error boundaries, such as **p3$_{1b}$** could also be formed but only as minor reaction channels. Since these resonantly stabilized C_6H_5 radicals are close in energy and within our experimental/theoretical error limits, we have to concede that our experiments alone cannot determine which isomer(s) is (are) formed under single collision conditions. We therefore solely refer to the underlying potential energy surfaces and RRKM theory calculations to elucidate the reaction mechanism. The RRKM calculations predict that 90% of C_6H_5 products are **p4$_{1b}$** plus atomic hydrogen, with the reaction starting from either of the three entrance channels **i4$_{1b}$**, **i5$_{1b}$** or **i8$_{1b}$**. The three reaction channels initiate with dicarbon binding to either acetyl carbon (**i5$_{1b}$**, **i8$_{1b}$**) or to both

(**i4$_{1b}$**). All addition pathways (**i5$_{1b}$**, **i8$_{1b}$**, **i4$_{1b}$**) eventually, via **i8$_{1b}$**, **i11$_{1b}$**, and **i10$_{1b}$**, reach **i9$_{1b}$** which emits a hydrogen atom from the central CH_2 group to form **p4$_{1b}$** through a tight exit transition state of 36 kJ mol^{-1} above the product. Small quantity of **p3$_{1b}$** and trace amounts of **p10$_{1b}$** and **p7$_{1b}$** are also predicted at the collision energy of 26 kJ mol^{-1}. Noteworthy that the major product predicted by RRKM calculations, **p4$_{1b}$** at -214 kJ mol^{-1}, provides a good match with the experimental reaction energy of 228 ± 31 kJ mol^{-1}.

The reaction of C_2 + 1,2-butadiene shows a reaction exoergicity of 213 ± 28 kJ mol^{-1}. The singlet surface reaction energy matches reasonably products **p3$_{bd}$**, **p4$_{bd}$**, and **p1$_{bd}$** plus atomic hydrogen, which have reaction energies of 225, 226, and 239 kJ mol^{-1}, respectively. On the singlet surface dicarbon adds to both ethyl carbons to form **i1$_{bd}$** in a barrierless addition, **i1$_{bd}$** isomerizes to **i2$_{bd}$** by insertion of the C_2 unit into the carbon chain and hydrogen emission from the CH group yields **p1$_{bd}$**, emission from the CH_2 group yields **p3$_{bd}$**, while emission from the methyl group yields **p4$_{bd}$**. All three hydrogen emissions pass loose transition states. RRKM theory however predicts that the major product *i*-C_5H_3 **p2$_{bd}$** (~85 %) results from the methyl group from **i3$_{bd}$**, but the branching ratios of the three C_6H_5 products are essentially almost equal. On the triplet surface C_6H_5 products **p1$_{bd}$**, **p3$_{bd}$**, **p4$_{bd}$**, **p8$_{bd}$**, **p9$_{bd}$**, and **p10$_{bd}$** lie in the exoergicity range of 199-251 kJ mol^{-1}, reasonably close to the energy bracket found under our experimental conditions of 213 ± 28 kJ mol^{-1}. The potential energy surface shows three addition channels are open to access these six products, either through barrier-less addition of dicarbon to C1, C2, or C3 of the acetyl group, to reach either intermediate **i6$_{bd}$**, **i3$_{bd}$**, or **i9$_{bd}$**, respectively. According to our RRKM calculations pathways leading from **i3$_{bd}$** predominantly produce the C_6H_5 product **p9$_{bd}$** plus atomic hydrogen. The reaction proceeds by hydrogen migration from the methyl group on **i3$_{bd}$** to the dicarbon unit to form **i4$_{bd}$** which subsequently emits a hydrogen atom from the non-terminal CH group to form **p9$_{bd}$** through a tight exit transition state. The second reaction pathway is initiated by dicarbon addition to the CH_2 group to form **i6$_{bd}$**. Intermediate **i6$_{bd}$** can undergo hydrogen migration from the methyl group to form **i8$_{bd}$** and subsequent hydrogen emission from the non-terminal CH group to yield **p8$_{bd}$** over a tight exit transition state. Formation of **p8$_{bd}$** plus atomic hydrogen is calculated to have a branching ratio of about 67% at the experimental collision energy. Also, from **i8$_{bd}$** formation of **p10$_{bd}$** plus atomic hydrogen is available through emission of a hydrogen atom from the central CH_2 group and has a branching ratio of 27%. The product **p4$_{bd}$** plus atomic

hydrogen is also produced by further isomerization from **i8$_{bd}$-i14$_{bd}$-i16$_{bd}$** and has a RRKM branching ratio of ~2%. A small reaction flux also proceeds from **i6$_{bd}$** to **i5$_{bd}$** and then to **i17$_{bd}$** and the latter decomposes producing a noticeable yield of *i*-C_5H_3 **p2$_{bd}$** + CH_3 (~4%) together with trace amounts of **p1$_{bd}$**, **p3$_{bd}$**, and **p4$_{bd}$**. The third reaction pathway begins with C_2 addition to the C3 carbon of 1,2-butadiene to form **i9$_{bd}$** and proceeds by four-member ring closure to **i13$_{bd}$**, which predominantly ring-opens to **i17$_{bd}$** resulting in a formal insertion of dicarbon into the C2-C3 bond of 1,2-butadiene. Intermediate **i17$_{bd}$** decomposes to four different products **p1$_{bd}$**, **p2$_{bd}$**, **p3$_{bd}$**, and **p4$_{bd}$**. According to the RRKM calculations, the methyl group loss dominates yielding 81% of *i*-C_5H_3 at the experimental collision energy, whereas the branching ratios of **p1$_{bd}$**, **p3$_{bd}$**, and **p4$_{bd}$** are 4.4, 7.6, and 7.0 %, respectively. If we consider only C_6H_5 products observable in experiment, the branching ratios of **p1$_{bd}$**, **p3$_{bd}$**, and **p4$_{bd}$** are 23, 40, and 37 %, respectively. Thus, the reaction outcome strongly depends on the site of the initial dicarbon attack; when C_2 adds to C1 or C2, mostly the **p8$_{bd}$**, **p9$_{bd}$**, **p10$_{bd}$** products exoergic by 199-209 kJ mol^{-1} are expected to form, but when C3 is attacked, more exoergic **p1$_{bd}$**, **p3$_{bd}$**, and **p4$_{bd}$** products (236-251 kJ mol^{-1}) are anticipated. Clearly, the **p8$_{bd}$**, **p9$_{bd}$**, **p10$_{bd}$** group better correlates with the experimental reaction energy which may be attributed to the fact that the C3 addition of dicarbon, though barrierless, is dynamically least favorable due to steric hindrance.

7. Summary

The reactions of dicarbon, C_2 ($X^1\Sigma_g^+/a^3\Pi_u$) with C_4H_6 isomers 2-butyne, 1-butyne and 1,2-butadiene were investigated at collision energies of about 26 kJ mol^{-1} using the cross molecular beam technique and supported by *ab initio* and RRKM calculations. The reactions all exhibit indirect scattering dynamics via complex formation through barrierless dicarbon addition pathways forming C_6H_5 products by dicarbon - atomic hydrogen exchange mechanisms. In the reaction of dicarbon plus 2-butyne, the singlet reaction proceeds by addition of dicarbon to the central acetyl carbons eventually forming 2,4-hexadiyne and subsequently emitting atomic hydrogen through a loose transition state from the methyl group to form **p1$_{2b}$** ($H_3CCCCCCH_2$) in an exoergic reaction by 218 ± 22 kJ mol^{-1}. The triplet dicarbon plus 2-butyne reaction was found to form products **p4$_{2b}$** ($H_3CC(C_2H)_2$) and **p1$_{2b}$**. In the singlet dicarbon reaction with 1-butyne,

dicarbon was found to bind to both acetyl carbons, isomerize and emit a hydrogen atom to form **p1$_{1b}$** ($H_3CCHCCCCH$) via a loose exit transition state and with a reaction exoergicity of 228 ± 31 kJ mol^{-1}. The triplet dicarbon plus 1-butyne reaction forms product **p4$_{1b}$** ($H_2CCHCCHCCH$) plus atomic hydrogen at branching ratios of 90% and experimental reaction exoergicity of 228 ± 31 kJ mol^{-1}. Product **p4$_{1b}$** is accessible by dicarbon addition to either acetyl carbon or to both to form addition complexes that isomerize and subsequently emit a hydrogen atom through a loose transition state.

The reaction of dicarbon plus 1,2-butadiene was found to be exoergic by 213 ± 28 kJ mol^{-1}. On the singlet surface the dicarbon addition occurs to both ethyl carbons to form **i1$_{bd}$** which isomerizes to fully insert the dicarbon and emits a hydrogen atom from various positions to form products **p1$_{bd}$** ($H_3CCCCCCH_2$, the same as **p1$_{2b}$**), **p3$_{bd}$** ($H_3CCHCCCCH$, the same as **p1$_{1b}$**) and **p4$_{bd}$** ($H_2CCHCCCCH_2$) with about equal branching ratios and without exit barriers. On the triplet surface three addition channels exist to form C_6H_5 products. Triplet dicarbon can bind to the C2 carbon of the ethyl chain to form **i3$_{bd}$** which binds to the C1 carbon to form **i4$_{bd}$** and emits a hydrogen atom forming **p9$_{bd}$** ($H_2CCC(CH_2)CCH$) with 90% branching ratio. Triplet dicarbon can also bind to the C1 carbon, in which case isomerization leads to products **p8$_{bd}$** (H_2CCCCH_2CCH) and **p10$_{bd}$** ($H_2CCHCCHCCH$, the same as **p4$_{1b}$**) through hydrogen loss with branching ratios of 67% and 27%, respectively. Finally, triplet C_2 can add to the C3 carbon and eventually produce **p1$_{bd}$**, **p3$_{bd}$**, and **p4$_{bd}$**. Meanwhile, although the methyl group loss channel was not observable in experiment, according to the present theoretical calculations, *i*-C_5H_3 + CH_3 should be the major products of the reactions of singlet dicarbon with 1-butyne and 1,2-butadiene. In a sharp contrast to the C_2 + 1,3-butadiene reaction studied by us earlier, the reactions of dicarbon with the other C_4H_6 isomers do not produce aromatic phenyl radicals. Detailed knowledge of the reaction mechanisms of dicarbon with C_4H_6 isomers 2-butyne, 1-butyne and 1,2-butadiene under combustion conditions are essential to chemical kinetic models to represent combustion process accurately. A common theme in modeling and analyzing combustion processes has been not to treat same mass isomers individually. We see here in the reaction of dicarbon ($X^1\Sigma_g^+/a^3\Pi_u$) with 2-butyne, 1-butyne and 1,2-butadiene over 10 different acyclic C_6H_5 and C_5H_3 RSFRs are formed highlighting the importance of isomer specific reaction mechanisms.

Acknowledgments

This work was supported by the US Department of Energy, Basic Energy Sciences (Grants No. DE-FG02-03ER15411 to RIK and the University of Hawaii and DE-FG02-04ER15570 to AMM at FIU).

Figure Captions

Figure 1. Reactive scattering signal in the reaction of dicarbon plus 2-butyne (CH_3CCCH_3 (X^1A_{1g})) monitored at m/z = 77 ($C_6H_5^+$). Laboratory frame data: (a) Angular distribution, black squares show integrated time-of-flight values, red line best fit. (b) Time-of-Flight spectra, open circles show raw data, and red line shows best fit to the data. Center-of-mass frame: (c) Center-of-mass angular distribution, (d) Product translational energy, hatched areas show error boundaries and red line depicts the 'best fit' function.

Figure 2. Reactive scattering signal in the reaction of dicarbon plus 1-butyne (CH_3CH_2CCH (X^1A')) monitored at m/z = 77 ($C_6H_5^+$). Laboratory frame data: (a) Angular distribution, black squares show integrated time-of-flight values, red line best fit. (b) Time-of-Flight spectra, open circles show raw data, and red line shows best fit to the data. Center-of-mass frame: (c) Center-of-mass angular distribution, (d) Product translational energy, hatched areas show error boundaries and red line depicts the 'best fit' function.

Figure 3. Reactive scattering signal in the reaction of dicarbon plus 1,2-butadiene (CH_3CHCCH_2 (X^1A')) monitored at m/z = 77 ($C_6H_5^+$). Laboratory frame data: (a) Angular distribution, black squares show integrated time-of-flight values, red line best fit. (b) Time-of-Flight spectra, open circles show raw data, and red line shows best fit to the data. Center-of-mass frame: (c) Center-of-mass angular distribution, (d) Product translational energy, hatched areas show error boundaries and red line depicts the 'best fit' function.

Figure 4. Schematic representation of the potential energy surface (PES) accessed via the reaction of dicarbon, ((a): singlet $X^1\Sigma_g^+$, (b): triplet $a^3\Pi_u$) plus 2-butyne (CH_3CCCH_3 (X^1A_{1g})) monitored at m/z = 77 ($C_6H_5^+$) at a collision energy of 26.4 kJ mol^{-1}. All energies are relative to reactants and in kJ mol^{-1}. Plain and bold numbers show relative energies computed at the CCSD(T)/CBS(dt) and CCSD(T)/CBS(dtq) levels of theory respectively. Most important reaction channels (according to RRKM calculations) on the triplet PES are shown in bold.

Figure 5. Schematic representation of the potential energy surface (PES) accessed via the reaction of dicarbon, ((a): singlet $X^1\Sigma_g^+$, (b): triplet $a^3\Pi_u$) plus 1-butyne ($HCCCH_2CH_3$ (X^1A_{1g})) monitored at m/z = 77 ($C_6H_5^+$) at a collision energy of 25.5 kJ mol^{-1}. All energies are relative to

reactants and in kJ mol^{-1}. Plain and bold numbers show relative energies computed at the CCSD(T)/CBS(dt) and CCSD(T)/CBS(dtq) levels of theory respectively. Most important reaction channels (according to RRKM calculations) on the triplet PES are shown in bold.

Figure 6. Schematic representation of the potential energy surface (PES) accessed via the reaction of dicarbon, ((a): singlet $X^1\Sigma_g^+$, (b): triplet $a^3\Pi_u$) plus 1,2-butadiene (CH_2CCHCH_3 (X^1A_{1g})) monitored at m/z = 77 ($C_6H_5^+$) at a collision energy of 24.9 kJ mol^{-1}. All energies are relative to reactants and in kJ mol^{-1}. Plain and bold numbers show relative energies computed at the CCSD(T)/CBS(dt) and CCSD(T)/CBS(dtq) levels of theory respectively. Most important reaction channels (according to RRKM calculations) on the triplet PES are shown in bold. The color specifies reaction channels initiated by C_2 addition to C1 (initial intermediate **i6$_{bd}$**, in blue), C2 (initial intermediate **i3$_{bd}$**, in red), and C3 (initial intermediate **i9$_{bd}$**, in green).

Figures

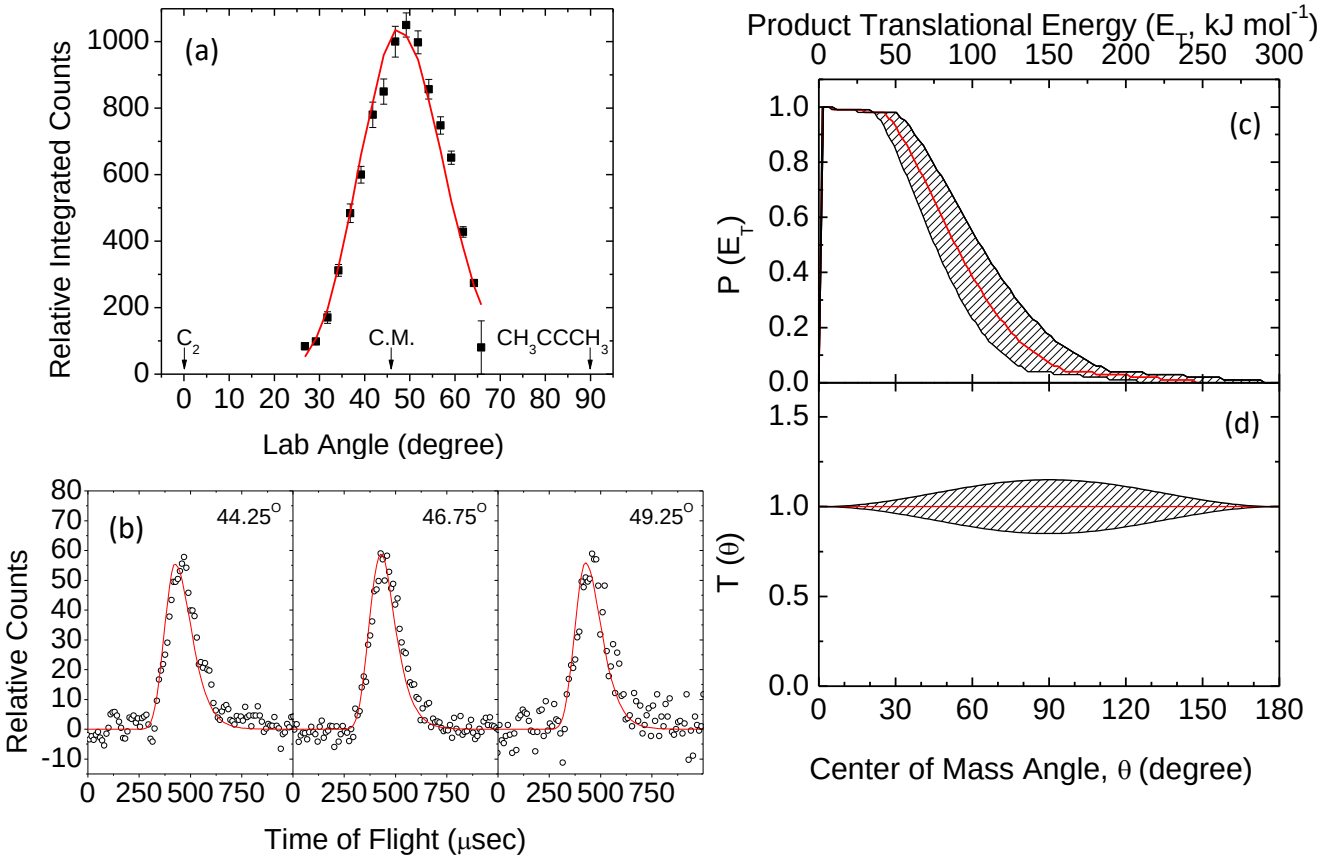

Figure 1

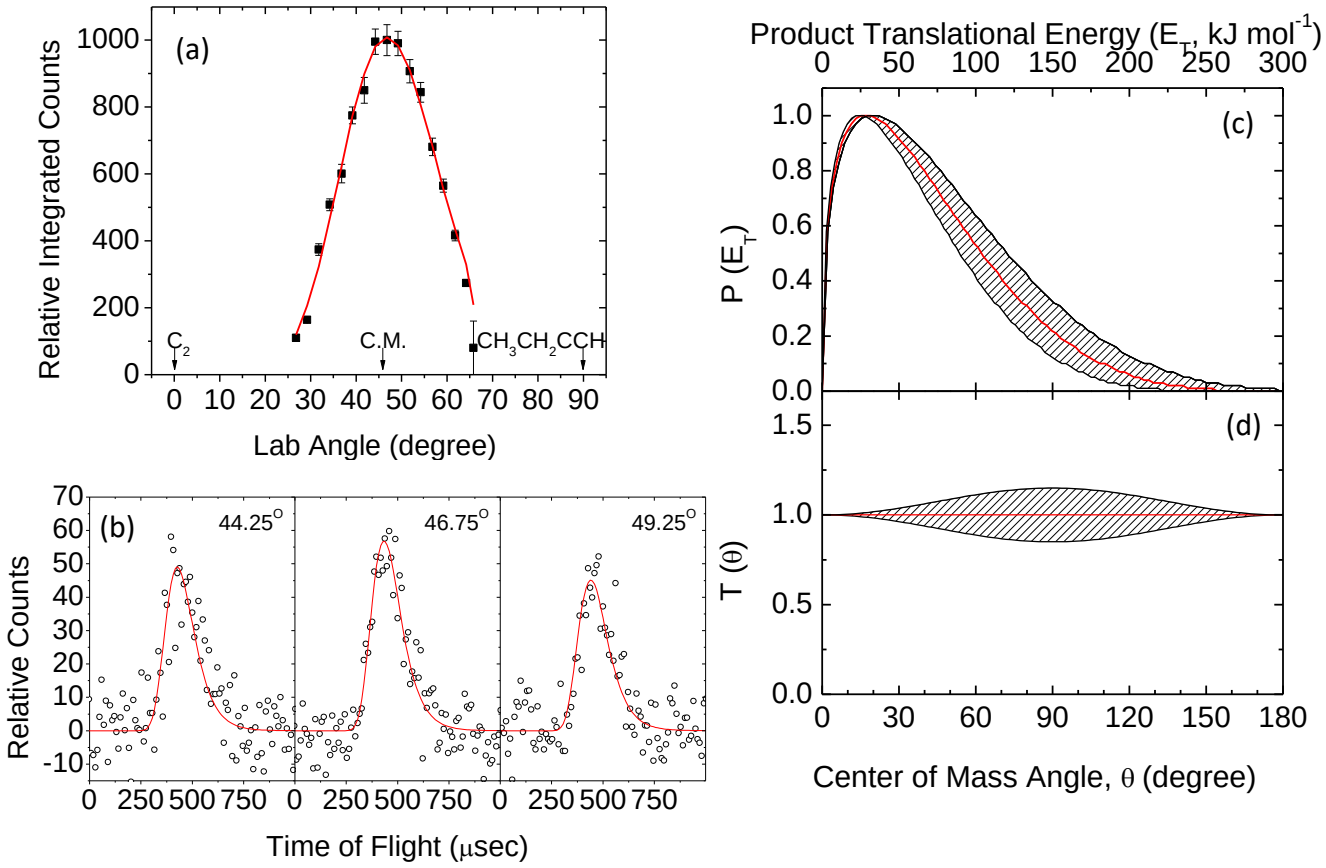
(a)
Relative Integrated Counts
Lab Angle (degree)
C2
C.M.
CH3CH2CCH
(b)
44.25°
46.75°
49.25°
Relative Counts
Time of Flight (μsec)
Product Translational Energy (ET, kJ mol-1)
(c)
P (ET)
(d)
T (θ)
Center of Mass Angle, θ (degree)

Figure 2

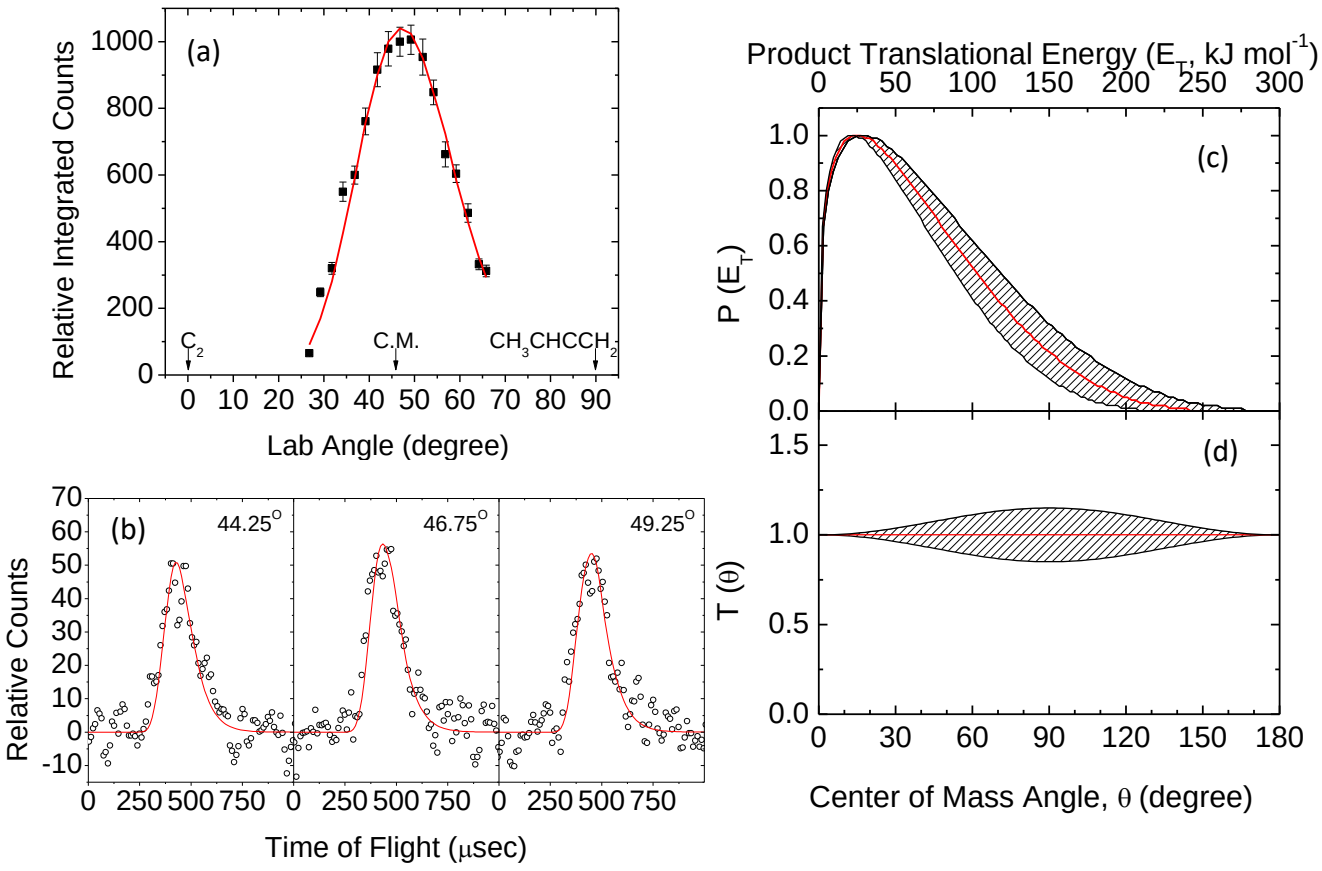
(a)
Relative Integrated Counts
1000
800
600
400
200
0
C2
C.M.
CH3CHCCH2
0 10 20 30 40 50 60 70 80 90
Lab Angle (degree)
(b)
44.25°
46.75°
49.25°
Relative Counts
70
60
50
40
30
20
10
0
-10
0 250 500 750 0 250 500 750 0 250 500 750
Time of Flight (μsec)
Product Translational Energy (ET, kJ mol-1)
0 50 100 150 200 250 300
(c)
P (ET)
1.0
0.8
0.6
0.4
0.2
0.0
(d)
T (θ)
1.5
1.0
0.5
0.0
0 30 60 90 120 150 180
Center of Mass Angle, θ (degree)

Figure 3

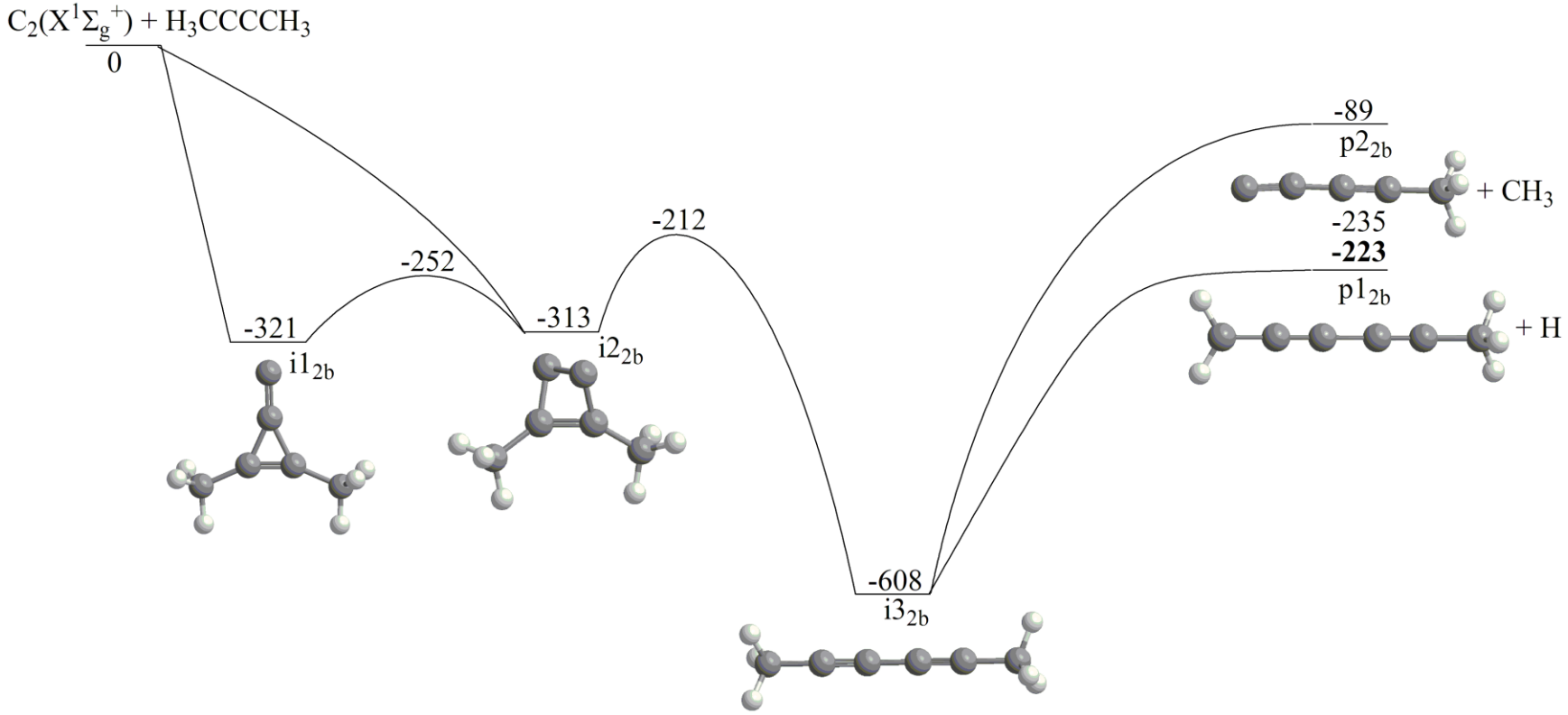
C2(X1Σg+) + H3CCCCH3
0
-321
i12b
-252
-313
i22b
-212
-608
i32b
-89
p22b
+ CH3
-235
-223
p12b
+ H

Figure 4(a)

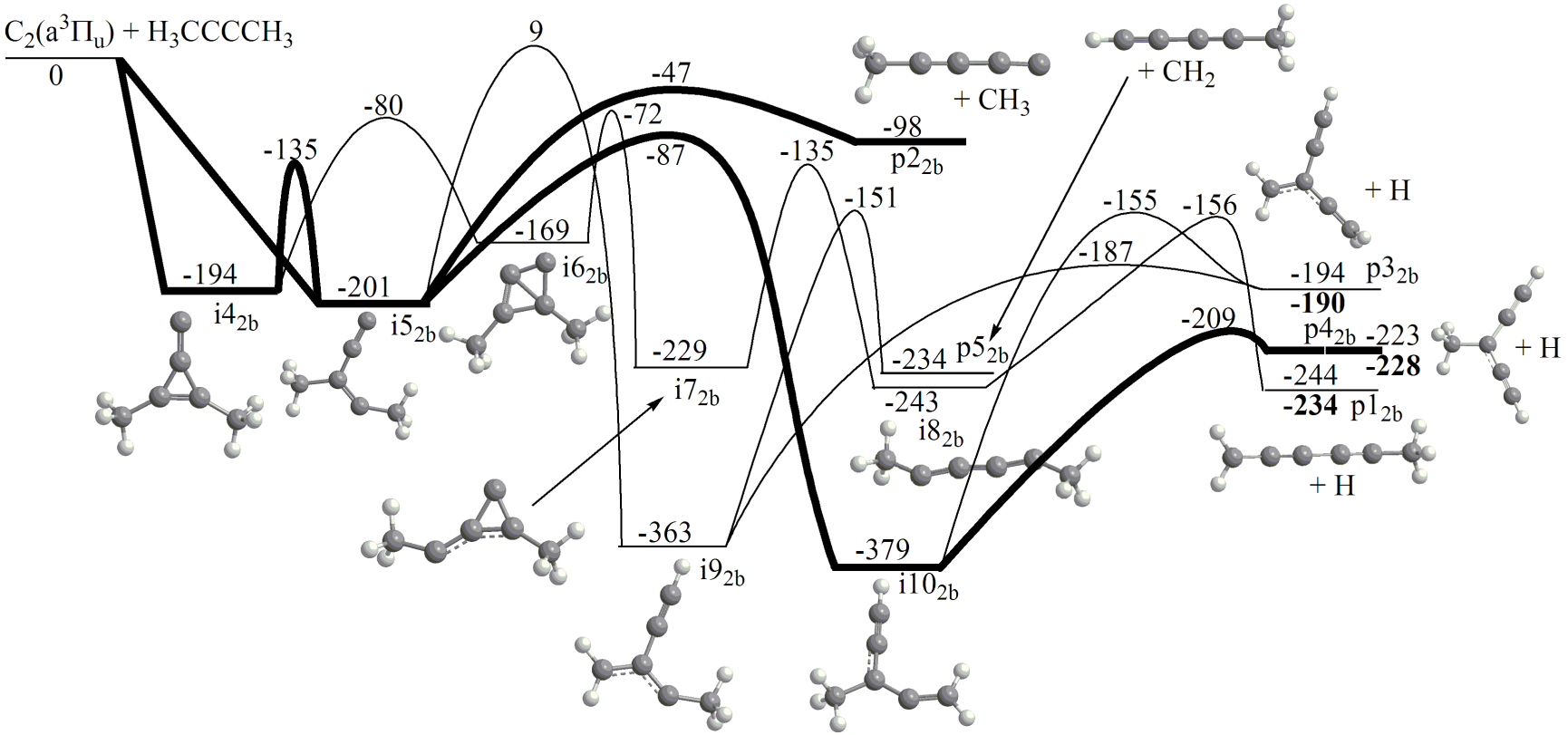
C2(a3Πu) + H3CCCCH3
0
-135
-80
9
-194
i4 2b
-201
i5 2b
-169
i6 2b
-47
-72
-87
-98
p2 2b
+ CH3
+ CH2
-135
-151
-155
-156
-187
+ H
-194 p3 2b
-190
-209
p4 2b -223
-228
-234 p5 2b
-244
-234 p1 2b
-243
i8 2b
+ H
+ H
-229
i7 2b
-363
i9 2b
-379
i10 2b

Figure 4(b)

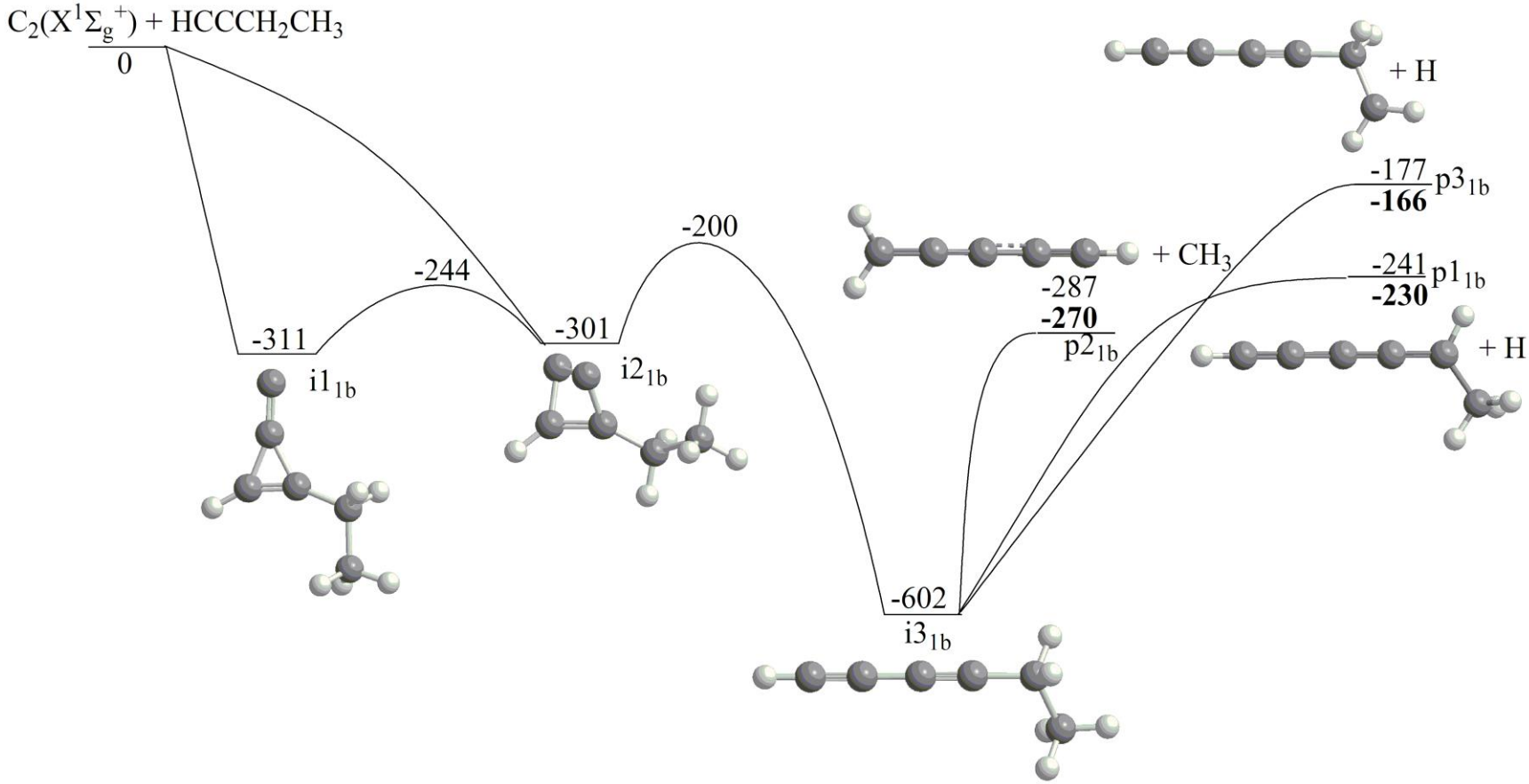
C2(X1Σg+) + HCCCH2CH3
0
-311
i11b
-244
-301
i21b
-200
-602
i31b
+ H
-177
-166
p31b
+ CH3
-287
-270
p21b
-241
-230
p11b
+ H

Figure 5(a)

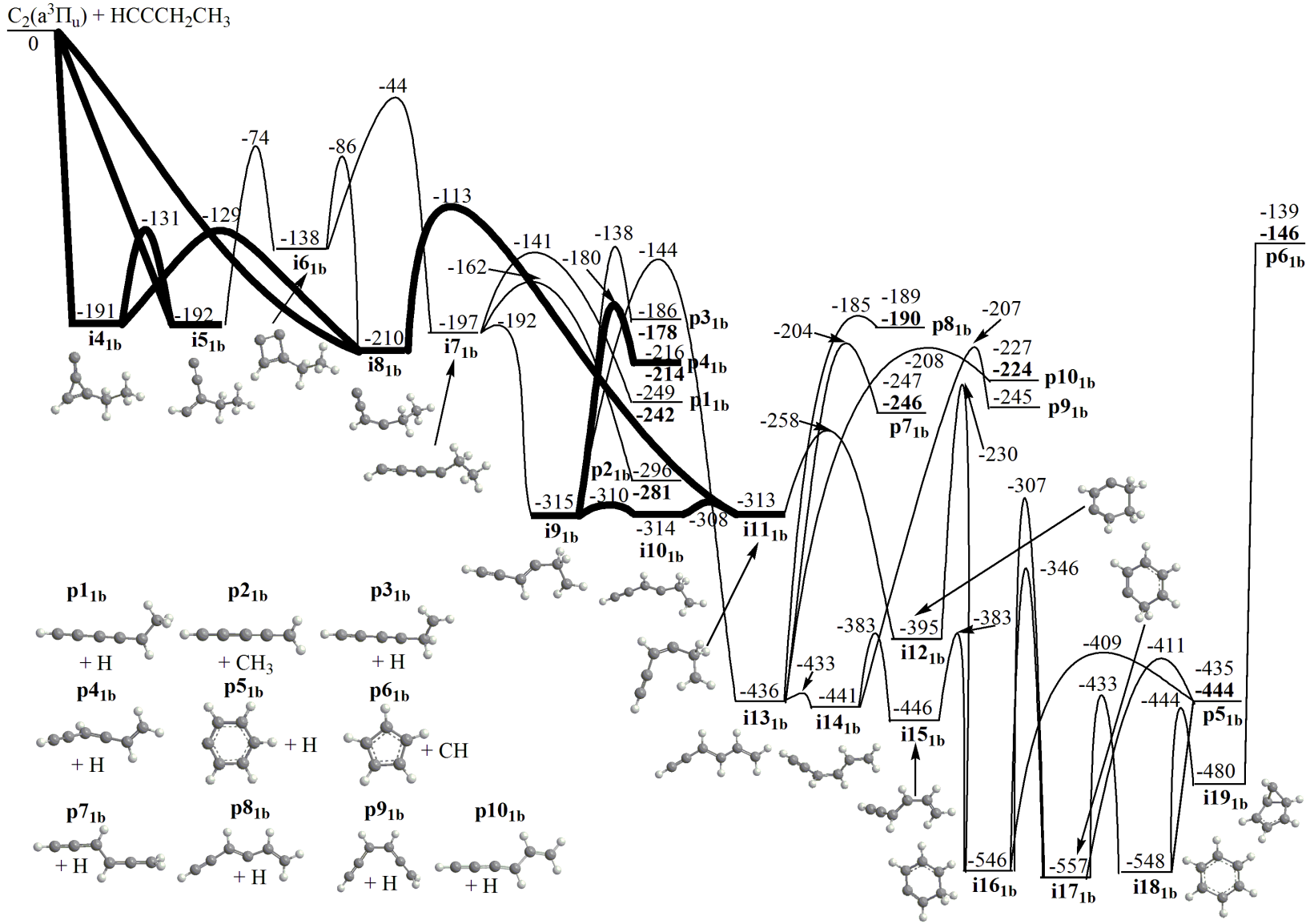
C2(a3Πu) + HCCCH2CH3
0
-191
i4 1b
-192
i5 1b
-74
-138
i6 1b
-86
-44
-131
-129
-210
i8 1b
-113
-162
-197
i7 1b
-192
-141
-180
-138
-144
-186
-178
p3 1b
-216
-214
p4 1b
-249
-242
p1 1b
p2 1b
-296
-281
-315
-310
i9 1b
-314
i10 1b
-308
-313
i11 1b
-204
-185
-189
-190
p8 1b
-207
-208
-247
-246
p7 1b
-227
-224
p10 1b
-245
p9 1b
-258
-230
-307
-346
-383
-395
i12 1b
-383
-409
-411
-433
-433
-436
-441
i13 1b
i14 1b
-446
i15 1b
-444
-435
-444
p5 1b
-480
i19 1b
-139
-146
p6 1b
-546
i16 1b
-557
i17 1b
-548
i18 1b
p1 1b
+ H
p2 1b
+ CH3
p3 1b
+ H
p4 1b
+ H
p5 1b
+ H
p6 1b
+ CH
p7 1b
+ H
p8 1b
+ H
p9 1b
+ H
p10 1b
+ H

Figure 5(b)

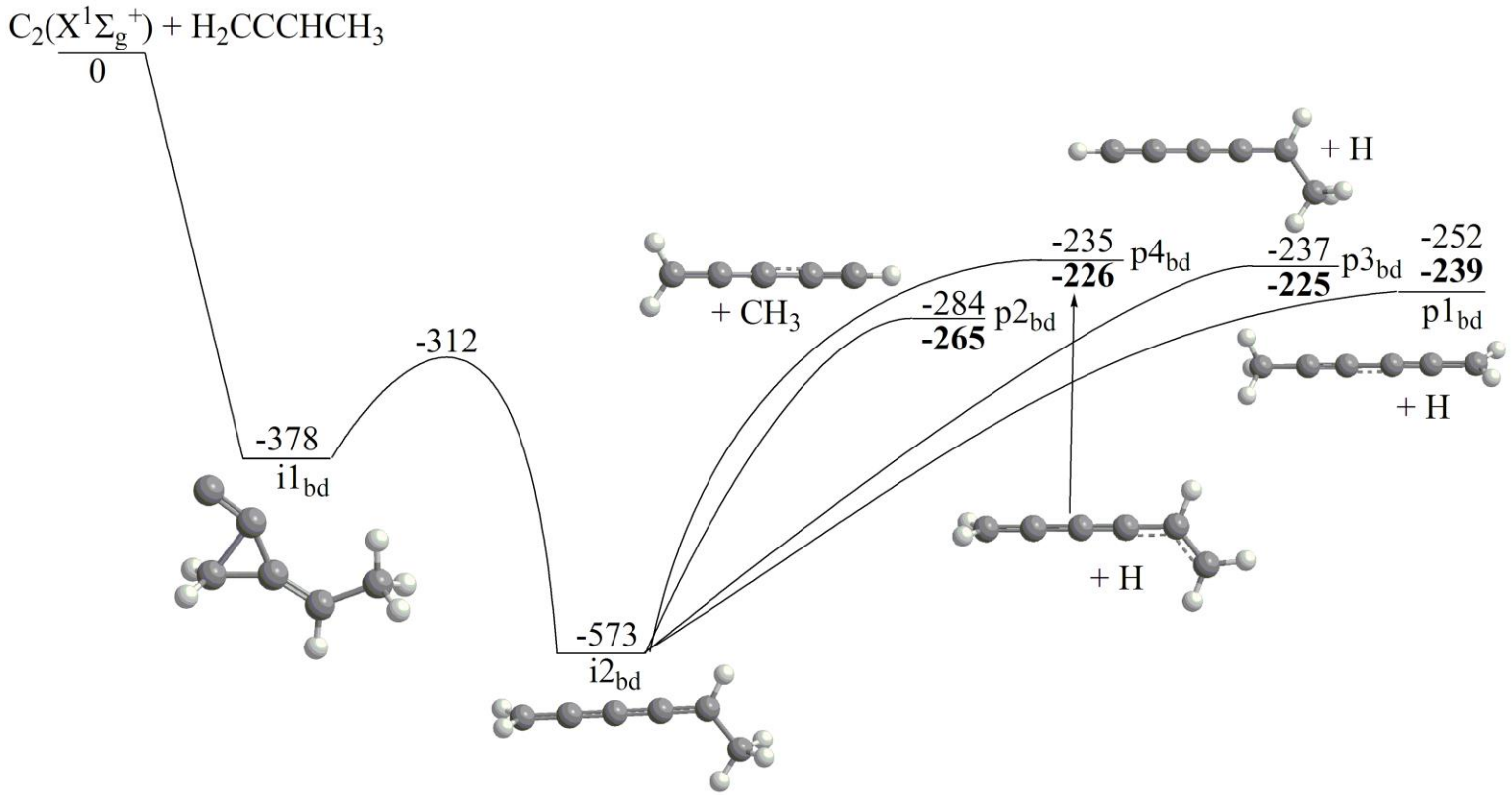
C2(X1Σg+) + H2CCCHCH3
0
-378
i1bd
-312
-573
i2bd
+ CH3
-284
-265
p2bd
-235
-226
p4bd
+ H
-237
-225
p3bd
-252
-239
p1bd
+ H
+ H

Figure 6(a)

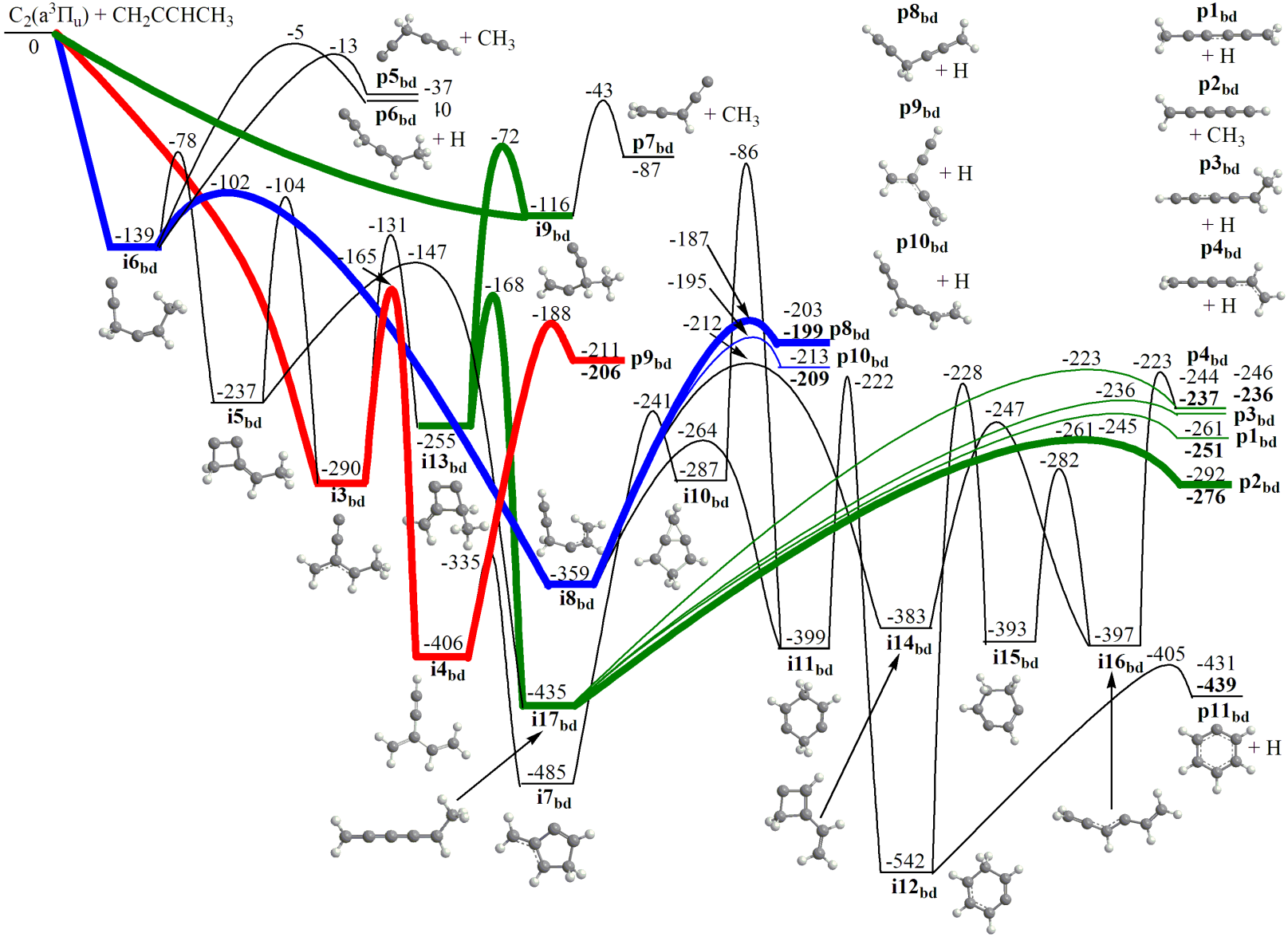
C2(a3Πu) + CH2CCHCH3
0
-5
-13
+ CH3
p5bd
-37
p6bd
+ H
-78
-102
-104
-139
i6bd
-131
-165
-147
-72
-116
i9bd
-43
+ CH3
p7bd
-87
-168
-188
-211
-206
p9bd
-237
i5bd
-290
i3bd
-255
i13bd
-335
-406
i4bd
-359
i8bd
-435
i17bd
-485
i7bd
-187
-195
-212
-86
-203
-199
p8bd
-213
p10bd
-209
-241
-264
-287
i10bd
-399
i11bd
-222
-383
i14bd
-542
i12bd
-228
-247
-393
i15bd
-282
-223
-223
-261
-245
-397
i16bd
-405
p8bd
+ H
p9bd
+ H
p10bd
+ H
p1bd
+ H
p2bd
+ CH3
p3bd
+ H
p4bd
+ H
-244
-246
-236
-237
p4bd
-236
p3bd
-261
p1bd
-251
-292
p2bd
-276
-431
-439
p11bd
+ H

Figure 6(b)

References

1. Frenklach, M., *Physical Chemistry Chemical Physics* **2002,** *4* (11), 2028-2037.
2. Cherchneff, I., *EAS Publ. Ser.* **2011,** *46* (PAHs and the Universe), 177-189.
3. Frenklach, M.; Feigelson, E. D., *Astrophys. J.* **1989,** *341* (1, Pt. 1), 372-84.
4. Frenklach, M.; Yuan, T.; Ramachandra, M. K., *Energy & Fuels* **1988,** *2* (4), 462-80.
5. Tielens, A. G. G. M., *Annu. Rev. Astron. Astrophys.* **2008,** *46*, 289-337.
6. Kaiser, R. I., *Chemical Reviews (Washington, D. C.)* **2002,** *102* (5), 1309-1358.
7. Hirota, T.; Ohishi, M.; Yamamoto, S., *Astrophys. J.* **2009,** *699* (1, Pt. 1), 585-602.
8. van Dishoeck, E. F., *Proc. Natl. Acad. Sci. U. S. A.* **2006,** *103* (33), 12249-12256.
9. Tielens, A. G. G. M.; van Kerckhoven, C.; Peeters, E.; Hony, S., *Symp. - Int. Astron. Union* **2000,** *197* (Astrochemistry: From Molecular Clouds to Planetary Systems), 349-362.
10. Allamandola, L. J., *EAS Publications Series* **2011,** *46* (PAHs and the Universe), 305-317.
11. Li, Y.; Tian, Z.; Zhang, L.; Yuan, T.; Zhang, K.; Yang, B.; Qi, F., *Proc. Combust. Inst.* **2009,** *32* (Pt. 1), 647-655.
12. Li, Y.; Zhang, L.; Tian, Z.; Yuan, T.; Wang, J.; Yang, B.; Qi, F., *Energy Fuels* **2009,** *23* (3), 1473-1485.
13. Li, Y.; Zhang, L.; Tian, Z.; Yuan, T.; Zhang, K.; Yang, B.; Qi, F., *Proc. Combust. Inst.* **2009,** *32* (Pt. 1), 1293-1300.
14. Li, Y.; Zhang, L.; Yuan, T.; Zhang, K.; Yang, J.; Yang, B.; Qi, F.; Law, C. K., *Combust. Flame* **2010,** *157* (1), 143-154.
15. Huang, C.; Zhang, F.; Kaiser, R. I.; Kislov, V. V.; Mebel, A. M.; Silva, R.; Gichuhi, W. K.; Suits, A. G., *Astrophysical Journal* **2010,** *714* (2, Pt. 1), 1249-1255.
16. Gu, X.; Guo, Y.; Zhang, F.; Mebel, A. M.; Kaiser, R. I., *Faraday Discussions* **2006,** *133* (Chemical Evolution of the Universe), 245-275.
17. Miller, J. A.; Klippenstein, S. J., *Journal of Physical Chemistry A* **2003,** *107* (39), 7783-7799.
18. Miller, J. A.; Melius, C. F., *Combustion and Flame* **1992,** *91* (1), 21-39.
19. Fahr, A.; Nayak, A., 32, 118, *Int. J. Chem. Kinet.* **2000,** *32*, 118-124.
20. Pousse, E.; Tian, Z. Y.; Glaude, P. A.; Fournet, R.; Battin-Leclerc, F., *Combust. Flame* **2010,** *157* (7), 1236-1260.
21. Kaiser, R. I.; Maksyutenko, P.; Ennis, C.; Zhang, F.; Gu, X.; Krishtal, S. P.; Mebel, A. M.; Kostko, O.; Ahmed, M., *Faraday Discuss.* **2010,** *147* (Chemistry of the Planets), 429-478.
22. Zhang, F.; Jones, B.; Maksyutenko, P.; Kaiser, R. I.; Chin, C.; Kislov, V. V.; Mebel, A. M., *J. Am. Chem. Soc.* **2010,** *132* (8), 2672-2683.
23. Jones, B. M.; Zhang, F.; Kaiser, R. I.; Jamal, A.; Mebel, A. M.; Cordiner, M. A.; Charnley, S. B., *Proc. Nat. Acad. Sci. U. S. A.* **2011,** *108* (2), 452-457, S452/1-S452/7.
24. Zhang, F.; Parker, D. S. N.; Kim, Y. S.; Kaiser, R. I.; Mebel, A. M., *Astrophys. J.* **2011,** *728* (2, Pt. 1), 141/1-141/10.
25. Richter, H.; Howard, J. B., *Prog. Energy Combust. Sci.* **2000,** *26* (4-6), 565-608.
26. *Faraday Discussion* **2001,** *119*.
27. Frenklach, M.; Wang, H., *Symp. (Int.) Combust., [Proc.]* **1991,** *23rd*, 1559-66.
28. Miller, J. A.; Pilling, M. J.; Troe, J., *Proc. Combust. Inst.* **2005,** *30* (Pt. 1), 43-88.

29. Kaiser, R. I.; Le, T. N.; Nguyen, T. L.; Mebel, A. M.; Balucani, N.; Lee, Y. T.; Stahl, F.; Schleyer, P. v. R.; Schaefer, H. F., III, *Faraday Discussions* **2001,** *119* (Combustion Chemistry: Elementary Reactions to Macroscopic Processes), 51-66.
30. Jones, B. M.; Zhang, F.; Kaiser, R. I.; Jamal, A.; Mebel, A. M.; Cordiner, M. A.; Charnley, S. B., *Proc. Natl. Acad. Sci. U. S. A.* **2011,** *108* (2), 452-457, S452/1-S452/7.
31. Kaiser, R. I.; Lee, Y. T.; Suits, A. G., *Journal of Chemical Physics* **1996,** *105* (19), 8705-8720.
32. Balucani, N.; Mebel, A. M.; Lee, Y. T.; Kaiser, R. I., *J. Phys. Chem. A* **2001,** *43*, 9813-9818.
33. Kaiser, R. I.; Stranges, D.; Lee, Y. T.; Suits, A. G., *Journal of Chemical Physics* **1996,** *105* (19), 8721-8733.
34. Kaiser, R. I.; Mebel, A. M.; Chang, A. H. H.; Lin, S. H.; Lee, Y. T., *J. Chem. Phys.* **1999,** *110*, 10330-10344
35. Guo, Y.; Gu, X.; Balucani, N.; Kaiser, R. I., *Journal of Physical Chemistry A* **2006,** *110* (19), 6245-6249.
36. Guo, Y.; Gu, X.; Zhang, F.; Mebel, A. M.; Kaiser, R. I., *Journal of Physical Chemistry A* **2006,** *110* (37), 10699-10707.
37. Parker, D. S. N.; Zhang, F.; Kim, Y. S.; Kaiser, R. I.; Mebel, A. M., *J. Phys. Chem. A* **2011,** *115* (5), 593-601.
38. Kaiser, R. I.; Stranges, D.; Bevsek, H. M.; Lee, Y. T.; Suits, A. G., *J. Chem. Phys.* **1997,** *106*, 4945-4953
39. Kaiser, R. I.; Nguyen, T. L.; Le, T. N.; Mebel, A. M., *Astrophysical Journal* **2001,** *561* (2, Pt. 1), 858-863.
40. Kaiser, R. I.; Goswami, M.; Maksyutenko, P.; Zhang, F.; Kim, Y. S., *J Phys Chem A* **2011,** *115*, 10251–10258.
41. Hidaka, Y.; Higashihara, T.; Ninomiya, N.; Oki, T.; Kawano, H., **1995,** *27*, 331–341.
42. Hidaka, Y.; Higashihara, T.; Ninomiya, N.; Oshita, H.; Kawano, H., *J. Phys. Chem.* **1993,** *97*, 10977–10983.
43. Miller, J. L.; Krisch, M. J.; Butler, L. J.; Shu, J., *J. Phys. Chem. A* **2005,** *109*, 4038-4048.
44. Melton, T. R.; Inal, F.; Senkan, S. M., *Combust. Flame* **2000,** *121* (4), 671-678.
45. El Bakali, A.; Braun-Unkhoff, M.; Dagaut, P.; Frank, P.; Cathonnet, M., *Proc. Combust. Inst.* **2000,** *28*, 1631-1638.
46. Zhang, F.; Jones, B.; Maksyutenko, P.; Kaiser, R. I.; Chin, C.; Kislov, V. V.; Mebel, A. M., *J. Am. Chem. Soc.* **2010,** *132* (8), 2672-2683.
47. Gu, X.; Guo, Y.; Kawamura, E.; Kaiser, R. I., *Journal of Vacuum Science & Technology, A: Vacuum, Surfaces, and Films* **2006,** *24* (3), 505-511.
48. Huang, L. C. L.; Lee, H. Y.; Mebel, A. M.; Lin, S. H.; Lee, Y. T.; Kaiser, R. I., *Journal of Chemical Physics* **2000,** *113* (21), 9637-9648.
49. Hahndorf, I.; Lee, H. Y.; Mebel, A. M.; Lin, S. H.; Lee, Y. T.; Kaiser, R. I., *J. Chem. Phys.* **2000,** *113* (21), 9622-9636.
50. Balucani, N.; Lee, H. Y.; Mebel, A. M.; Lee, Y. T.; Kaiser, R. I., *Journal of Chemical Physics* **2001,** *115* (11), 5107-5116.
51. Guo, Y.; Gu, X.; Zhang, F.; Mebel, A. M.; Kaiser, R. I., *J. Phys. Chem. A* **2006,** *110* (37), 10699-10707.
52. Becke, A. D. *J. Chem. Phys.* **1993**, *98*, 5648-5652.

53. Lee, C.; Yang, W.; Parr, R. G. *Phys. Rev. B* **1988**, *37*, 785-789.
54. Purvis, G. D.; Bartlett, R. J. *J. Chem. Phys.* **1982**, *76*, 1910-1918.
55. Dunning, Jr., T. H. *J. Chem. Phys.* **1989**, *90*, 1007-1023.
56. Huh, S. B.; Lee, J. S. *J. Chem. Phys.* **2003**, *118*, 3035-3042.
57. Frisch, M. J.; Trucks, G. W.; Schlegel ,H. B. et al., GAUSSIAN 09, Revision A.1 Gaussian, Inc., Wallingford, CT, 2009.
58. MOLPRO, version 2010.1, a package of ab initio programs, Werner, H.-J.; Knowles, P. J.; Knizia, G.; Manby, F. R.; Schütz, M. and others, see http://www.molpro.net.
59. Robinson, P. J.; Holbrook, K. A. Unimolecular Reactions (Wiley, New York, 1972); Eyring, H.; Lin, S. H.; Lin, S. M.Basic Chemical Kinetics (Wiley, New York, 1980); Steinfield, J.; Francisco, J.; Hase, W. Chemical Kinetics and Dynamics (Prentice Hall, Englewood Cliffs, NJ, 1989).
60. Kislov, V. V.; Nguyen, T. L.; Mebel, A. M.; Lin, S. H.; Smith, S. C. *J. Chem. Phys.* **2004**, *120*, 7008.
61. Guo, Y.; Gu, X.; Zhang, F.; Mebel, A. M.; Kaiser, R. I., *Phys. Chem. Chem. Phys.* **2007,** *9* (16), 1972-1979.
62. Kaiser, R. I.; Lee, H. Y.; Mebel, A. M.; Lee, Y. T., *Astrophys. J* **2001,** *548*, 852-860.
63. Levine, R. D., *Molecular Reaction Dynamics* **2005**.

Electronic Supplementary Information (ESI)

for

Understanding the Chemical Dynamics of the Reactions of Dicarbon with 1-Butyne, 2-Butyne, and 1,2-Butadiene – Toward the Formation of Resonantly Stabilized Free Radicals

by

Dorian S. N. Parker, S. Maity, Beni B. Dangi, Ralf I. Kaiser*

Department of Chemistry, University of Hawai'i at Manoa, Honolulu, HI 96822

Alexander Landera, A. M. Mebel*

Department of Chemistry & Biochemistry, Florida International University, Miami, FL 33199

Table S1. Rate constants for various individual unimolecular reaction steps calculated using RRKM theory under single-collision conditions at different collision energies.

(a) $C_2(X^1\Sigma_g^+)$ + 2-butyne, Figure 4(a). RRKM calculations were not performed since product **p1$_{2b}$** is the only C_6H_5 isomer able to be formed on the singlet surface.

(b) $C_2(a^3\Pi_u)$ + 2-butyne, Figure 4(b).

		Collision Energy, kJ mol^{-1}						
From	To	0	5	10	15	20	26.4	30
i4$_{2b}$	**i5$_{2b}$**	3.10E+11	3.45E+11	3.82E+11	4.21E+11	4.60E+11	5.20E+11	5.53E+11
i5$_{2b}$	**i4$_{2b}$**	3.60E+10	4.05E+10	4.50E+10	4.99E+10	5.52E+10	6.24E+10	6.66E+10
i4$_{2b}$	**i6$_{2b}$**	1.93E+08	2.55E+08	3.30E+08	4.22E+08	5.33E+08	7.06E+08	8.21E+08
i6$_{2b}$	**i4$_{2b}$**	1.14E+09	1.45E+09	1.82E+09	2.26E+09	2.76E+09	3.52E+09	4.01E+09
i5$_{2b}$	**i9$_{2b}$**	0.00E+00	0.00E+00	2.06E+00	8.38E+00	2.86E+01	1.11E+02	2.18E+02
i9$_{2b}$	**i5$_{2b}$**	0.00E+00	0.00E+00	8.37E-05	3.83E-04	1.47E-03	6.58E-03	1.40E-02
i5$_{2b}$	**i10$_{2b}$**	2.81E+07	3.57E+07	4.49E+07	5.59E+07	6.88E+07	8.86E+07	1.01E+08
i10$_{2b}$	**i5$_{2b}$**	4.51E+02	6.55E+02	9.39E+02	1.33E+03	1.85E+03	2.77E+03	3.46E+03
i5$_{2b}$	**p2$_{2b}$**	5.60E+06	1.02E+07	1.78E+07	2.96E+07	4.75E+07	8.32E+07	1.12E+08
i6$_{2b}$	**i7$_{2b}$**	4.83E+08	6.43E+08	8.42E+08	1.08E+09	1.37E+09	1.83E+09	2.12E+09
i7$_{2b}$	**i6$_{2b}$**	1.09E+06	1.56E+06	2.20E+06	3.02E+06	4.10E+06	5.91E+06	7.19E+06
i7$_{2b}$	**i8$_{2b}$**	4.66E+09	5.39E+09	6.19E+09	7.07E+09	8.03E+09	9.39E+09	1.02E+10
i8$_{2b}$	**i7$_{2b}$**	1.08E+09	1.26E+09	1.47E+09	1.69E+09	1.94E+09	2.31E+09	2.53E+09
i8$_{2b}$	**p1$_{2b}$**	5.73E+11	6.54E+11	7.44E+11	8.42E+11	9.49E+11	1.10E+12	1.19E+12

i9$_{2b}$	**p3$_{2b}$**	3.99E+09	4.75E+09	5.62E+09	6.61E+09	7.75E+09	9.44E+09	1.05E+10
i9$_{2b}$	**p5$_{2b}$**	5.73E+08	7.22E+08	9.04E+08	1.12E+09	1.39E+09	1.80E+09	2.07E+09
i10$_{2b}$	**p3$_{2b}$**	5.37E+07	6.78E+07	8.48E+07	1.05E+08	1.30E+08	1.69E+08	1.95E+08
i10$_{2b}$	**p4$_{2b}$**	6.52E+10	7.57E+10	8.74E+10	1.01E+11	1.15E+11	1.37E+11	1.50E+11

(c) $C_2(X^1\Sigma_g^+)$ + 1-butyne, Figure 5(a).

		Collision Energy, kJ mol^{-1}					
From	To	0	4.18	8.37	12.55	16.74	22.00
i2$_{1b}$	**i3$_{1b}$**	6.22E+10	6.69E+10	7.18E+10	7.69E+10	8.24E+10	8.95E+10
i3$_{1b}$	**i2$_{1b}$**	5.87E+04	6.91E+04	8.19E+04	9.62E+04	1.13E+05	1.35E+05
i3$_{1b}$	**p2$_{1b}$**	1.59E+10	1.69E+10	1.80E+10	1.91E+10	2.02E+10	2.16E+10
i3$_{1b}$	**p1$_{1b}$**	9.55E+08	1.04E+09	1.14E+09	1.24E+09	1.35E+09	1.50E+09
i3$_{1b}$	**p3$_{1b}$**	1.13E+07	1.31E+07	1.50E+07	1.73E+07	1.99E+07	2.35E+08

(d) $C_2(a^3\Pi_u)$ + 1-butyne, Figure 5(b).

		Collision Energy, kJ mol^{-1}					
From	To	0	4.18	8.37	12.55	16.74	22.00
i8$_{1b}$	**i11$_{1b}$**	4.39E+07	5.09E+07	5.87E+07	6.73E+07	7.69E+07	9.03E+07
i11$_{1b}$	**i8$_{1b}$**	1.49E+04	1.85E+04	2.28E+04	2.78E+04	3.39E+04	4.30E+04
i8$_{1b}$	**i6$_{1b}$**	9.91E+02	1.55E+03	2.32E+03	3.40E+03	4.87E+03	7.45E+03
i11$_{1b}$	**i12$_{1b}$**	2.96E+09	3.06E+09	3.16E+09	3.26E+09	3.36E+09	3.49E+09
i12$_{1b}$	**i11$_{1b}$**	7.34E+10	7.93E+10	8.55E+10	9.21E+10	9.90E+10	1.08E+11
i11$_{1b}$	**i10$_{1b}$**	2.86E+12	2.87E+12	2.88E+12	2.89E+12	2.91E+12	2.91E+12
i10$_{1b}$	**i11$_{1b}$**	5.19E+12	5.21E+12	5.23E+12	5.25E+12	5.27E+12	5.29E+12
i12$_{1b}$	**i16$_{1b}$**	1.70E+09	1.87E+09	2.05E+09	2.24E+09	2.47E+09	2.74E+09
i16$_{1b}$	**i12$_{1b}$**	3.75E+06	4.30E+06	4.91E+06	5.61E+06	6.38E+06	7.48E+06
i16$_{1b}$	**i17$_{1b}$**	3.47E+09	3.70E+09	3.95E+09	4.21E+09	4.48E+09	4.84E+09
i17$_{1b}$	**i16$_{1b}$**	2.83E+09	3.02E+09	3.23E+09	3.45E+09	3.68E+09	3.99E+09
i16$_{1b}$	**p5$_{1b}$**	1.56E+11	1.63E+11	1.70E+11	1.77E+11	1.84E+11	1.93E+11
i17$_{1b}$	**i18$_{1b}$**	1.82E+13	1.81E+13	1.80E+13	1.79E+13	2.11E+13	2.21E+13
i18$_{1b}$	**i17$_{1b}$**	4.84E+10	4.99E+10	5.17E+10	5.34E+10	5.51E+10	5.73E+10
i17$_{1b}$	**p5$_{1b}$**	1.66E+11	1.73E+11	1.81E+11	1.88E+11	1.96E+11	2.06E+11
i18$_{1b}$	**i19$_{1b}$**	5.88E+08	6.04E+08	6.20E+08	6.36E+08	6.53E+08	6.73E+08
i19$_{1b}$	**i18$_{1b}$**	4.15E+12	4.20E+12	4.25E+12	4.30E+12	4.34E+12	4.40E+12
i18$_{1b}$	**p5$_{1b}$**	2.07E+08	2.16E+08	2.25E+08	2.35E+08	2.44E+08	2.57E+08
i19$_{1b}$	**p6$_{1b}$**	3.55E+06	4.45E+06	5.55E+06	6.88E+06	8.49E+06	1.10E+07
i10$_{1b}$	**i9$_{1b}$**	1.82E+12	1.83E+12	1.83E+12	1.83E+12	1.84E+12	1.84E+12
i9$_{1b}$	**i10$_{1b}$**	3.12E+12	3.13E+12	3.14E+12	3.15E+12	3.16E+12	3.18E+12

i9$_{1b}$	**i7$_{1b}$**	2.78E+08	3.06E+08	3.36E+08	3.68E+08	4.03E+08	4.49E+08
i7$_{1b}$	**i9$_{1b}$**	5.40E+11	5.49E+11	5.59E+11	5.68E+11	5.78E+11	5.89E+11
i9$_{1b}$	**i13$_{1b}$**	3.26E+07	3.87E+07	4.58E+07	5.39E+07	6.32E+07	7.66E+07
i13$_{1b}$	**i9$_{1b}$**	6.23E+04	7.79E+04	9.69E+04	1.20E+05	1.48E+05	1.90E+05
i9$_{1b}$	**p3$_{1b}$**	5.84E+08	7.18E+08	8.77E+08	1.07E+09	1.29E+09	1.62E+09
i7$_{1b}$	**i6$_{1b}$**	2.08E+03	3.18E+03	4.73E+03	6.86E+03	9.70E+03	1.47E+04
i6$_{1b}$	**i7$_{1b}$**	3.09E+06	4.35E+06	5.96E+06	8.02E+06	1.06E+07	1.46E+07
i7$_{1b}$	**p2$_{1b}$**	2.30E+12	2.49E+12	2.67E+12	2.86E+12	3.06E+12	3.33E+12
i7$_{1b}$	**p1$_{1b}$**	2.54E+11	2.84E+11	3.15E+11	3.49E+11	3.86E+11	4.35E+11
i6$_{1b}$	**i5$_{1b}$**	2.11E+10	2.53E+10	3.00E+10	3.52E+10	4.10E+10	4.91E+10
i5$_{1b}$	**i6$_{1b}$**	5.56E+07	7.06E+07	9.11E+07	1.15E+08	1.43E+08	1.85E+08
i5$_{1b}$	**i4$_{1b}$**	3.52E+10	3.88E+10	4.26E+10	4.67E+10	5.09E+10	5.66E+10
i4$_{1b}$	**i5$_{1b}$**	6.04E+10	6.70E+10	7.33E+10	8.03E+10	8.77E+10	9.76E+10
i13$_{1b}$	**i4$_{1b}$**	1.63E+12	1.63E+12	1.63E+12	1.63E+12	1.63E+12	1.63E+12
i14$_{1b}$	**i13$_{1b}$**	2.57E+12	2.58E+12	2.58E+12	2.59E+12	2.60E+12	2.60E+12
i13$_{1b}$	**p8$_{1b}$**	6.85E+06	8.17E+06	9.70E+06	1.15E+07	1.35E+07	1.68E+07
i13$_{1b}$	**p10$_{1b}$**	3.82E+07	4.42E+07	5.10E+07	5.88E+07	6.73E+07	7.97E+07
i14$_{1b}$	**i15$_{1b}$**	3.95E+11	4.04E+11	4.13E+11	4.23E+11	4.32E+11	4.44E+11
i15$_{1b}$	**i14$_{1b}$**	3.67E+11	3.76E+11	3.84E+11	3.94E+11	4.03E+11	4.14E+11
i15$_{1b}$	**p7$_{1b}$**	3.44E+07	3.99E+07	4.62E+07	5.33E+07	6.13E+07	7.29E+07
i15$_{1b}$	**p9$_{1b}$**	8.39E+06	9.98E+06	1.19E+07	1.41E+07	1.66E+07	2.03E+07

(e) $C_2(X^1\Sigma_g^+)$ + 1,2-butadiene, Figure 6(a).

		Collision Energy, kJ mol^{-1}					
From	To	0	4.18	8.37	12.55	16.74	22.00
i1$_{bd}$	**i2$_{bd}$**	3.88E+10	4.07E+10	4.25E+10	4.43E+10	4.62E+10	4.84E+10
i2$_{bd}$	**i1$_{bd}$**	3.90E+06	4.30E+06	4.74E+06	5.20E+06	5.71E+06	6.37E+06
i2$_{bd}$	**p1$_{bd}$**	3.13E+08	3.42E+08	3.73E+08	4.07E+08	4.43E+08	4.92E+08
i2$_{bd}$	**p2$_{bd}$**	4.24E+09	4.57E+09	4.92E+09	5.29E+09	5.68E+09	6.21E+09
i2$_{bd}$	**p3$_{bd}$**	4.09E+08	4.49E+08	4.92E+08	5.39E+08	5.90E+08	6.59E+08
i2$_{bd}$	**p4$_{bd}$**	4.70E+08	5.13E+08	5.60E+08	6.11E+08	6.65E+08	7.39E+08

(f) $C_2(a^3\Pi_u)$ + 1,2-butadiene, Figure 6(b).

		Collision Energy, kJ mol^{-1}					
From	To	0	4.18	8.37	12.55	16.74	22.00
i6$_{bd}$	**i8$_{bd}$**	5.16E+10	5.62E+10	6.09E+10	6.57E+10	7.07E+10	7.74E+10
i8$_{bd}$	**i6$_{bd}$**	3.95E+03	5.18E+03	6.73E+03	8.68E+03	1.11E+04	1.50E+04
i6$_{bd}$	**i5$_{bd}$**	1.73E+09	2.02E+09	2.34E+09	2.69E+09	3.06E+09	3.58E+09

i5$_{bd}$	**i6$_{bd}$**	2.48E+07	3.27E+07	4.25E+07	5.47E+07	6.96E+07	9.32E+07
i5$_{bd}$	**i17$_{bd}$**	4.34E+10	4.83E+10	5.36E+10	5.93E+10	6.52E+10	7.37E+10
i17$_{bd}$	**i5$_{bd}$**	1.60E+04	1.96E+04	2.39E+04	2.89E+04	3.48E+04	4.38E+04
i6$_{bd}$	**p6$_{bd}$**	4.75E+02	2.39E+03	8.71E+03	2.56E+04	6.48E+04	1.78E+05
i6$_{bd}$	**p5$_{bd}$**	2.60E+04	9.21E+04	2.66E+05	6.63E+05	1.49E+06	3.64E+06
i8$_{bd}$	**i11$_{bd}$**	5.45E+08	5.76E+08	6.09E+08	6.42E+08	6.77E+08	7.22E+08
i11$_{bd}$	**i8$_{bd}$**	3.81E+10	4.09E+10	4.39E+10	4.72E+10	5.05E+10	5.50E+10
i8$_{bd}$	**i14$_{bd}$**	1.75E+08	1.93E+08	2.11E+08	2.32E+08	2.54E+08	2.83E+08
i14$_{bd}$	**i8$_{bd}$**	4.63E+09	5.17E+09	5.74E+09	6.37E+09	7.06E+09	7.99E+09
i8$_{bd}$	**p10$_{bd}$**	2.41E+09	2.75E+09	3.12E+09	3.54E+09	3.99E+09	4.64E+09
i8$_{bd}$	**p8$_{bd}$**	5.62E+09	6.48E+09	7.45E+09	8.53E+09	9.74E+09	1.15E+10
i11$_{bd}$	**i12$_{bd}$**	2.01E+10	2.23E+10	2.46E+10	2.71E+10	2.98E+10	3.36E+09
i12$_{bd}$	**i11$_{bd}$**	1.75E+06	2.02E+06	2.32E+06	2.66E+06	3.04E+06	3.59E+06
i11$_{bd}$	**i10$_{bd}$**	2.81E+03	3.88E+03	5.25E+03	7.07E+03	9.41E+03	1.33E+04
i10$_{bd}$	**i11$_{bd}$**	3.62E+05	4.71E+05	6.07E+05	7.73E+05	9.79E+05	1.30E+06
i12$_{bd}$	**i15$_{bd}$**	3.59E+06	4.12E+06	4.71E+06	5.38E+06	6.12E+06	7.19E+06
i15$_{bd}$	**i12$_{bd}$**	2.40E+09	3.62E+09	3.98E+09	4.36E+09	4.76E+09	5.32E+09
i12$_{bd}$	**p11$_{bd}$**	3.10E+11	3.23E+11	3.36E+11	3.51E+11	3.64E+11	3.83E+11
i14$_{bd}$	**i16$_{bd}$**	3.81E+10	4.12E+10	4.44E+10	4.79E+10	5.16E+10	5.65E+10
i16$_{bd}$	**i14$_{bd}$**	3.23E+08	3.49E+08	3.78E+08	4.09E+08	4.41E+08	4.84E+08
i16$_{bd}$	**i15$_{bd}$**	2.06E+08	2.17E+08	2.30E+08	2.43E+08	2.56E+08	2.74E+08
i15$_{bd}$	**i16$_{bd}$**	8.57E+10	9.08E+10	9.61E+10	1.02E+11	1.07E+11	1.15E+11
i16$_{bd}$	**p4$_{bd}$**	9.21E+09	1.03E+10	1.16E+10	1.29E+10	1.44E+10	1.65E+10
i7$_{bd}$	**i4$_{bd}$**	9.74E+10	1.04E+11	1.10E+11	1.17E+11	1.23E+11	1.32E+11
i4$_{bd}$	**i7$_{bd}$**	3.61E+10	3.72E+10	3.83E+10	3.94E+10	4.05E+10	4.18E+10
i7$_{bd}$	**i10$_{bd}$**	6.15E+07	6.89E+07	7.70E+07	8.59E+07	9.57E+07	1.09E+08
i10$_{bd}$	**i7$_{bd}$**	1.09E+12	1.13E+12	1.17E+12	1.21E+12	1.25E+12	1.30E+12
i3$_{bd}$	**i4$_{bd}$**	1.02E+09	1.15E+09	1.30E+09	1.46E+09	1.63E+09	1.88E+09
i4$_{bd}$	**i3$_{bd}$**	5.74E+05	6.83E+05	8.09E+05	9.55E+05	1.12E+06	1.37E+06
i3$_{bd}$	**i13$_{bd}$**	2.78E+07	3.24E+07	3.76E+07	4.35E+07	5.00E+07	5.93E+07
i3$_{bd}$	**i5$_{bd}$**	9.08E+05	1.15E+06	1.43E+06	1.78E+06	2.17E+06	2.76E+06
i5$_{bd}$	**i3$_{bd}$**	1.29E+08	1.60E+08	1.97E+08	2.40E+08	2.91E+08	3.68E+08
i4$_{bd}$	**p9$_{bd}$**	4.76E+07	5.69E+07	6.79E+07	8.05E+07	9.54E+07	1.17E+08
i9$_{bd}$	**i13$_{bd}$**	8.82E+09	1.02E+10	1.16E+10	1.32E+10	1.50E+10	1.73E+10
i13$_{bd}$	**i9$_{bd}$**	2.85E+06	3.91E+06	5.29E+06	7.06E+06	9.30E+06	1.30E+07
i9$_{bd}$	**p7$_{bd}$**	1.16E+09	1.78E+09	2.64E+09	3.79E+09	5.30E+09	7.84E+09
i13$_{bd}$	**i17$_{bd}$**	1.06E+11	1.17E+11	1.28E+11	1.40E+11	1.52E+11	1.69E+11
i17$_{bd}$	**i13$_{bd}$**	3.90E+04	4.65E+04	5.52E+04	6.52E+04	7.68E+04	9.38E+04
i17$_{bd}$	**p1$_{bd}$**	2.46E+09	2.75E+09	3.06E+09	3.38E+09	3.75E+09	4.25E+09
i17$_{bd}$	**p2$_{bd}$**	4.90E+10	5.39E+10	5.92E+10	6.47E+10	7.09E+10	7.91E+10
i17$_{bd}$	**p3$_{bd}$**	4.06E+09	4.57E+09	5.12E+09	5.76E+09	6.40E+09	7.33E+09
i17$_{bd}$	**p4$_{bd}$**	3.53E+09	4.01E+09	4.57E+09	5.15E+09	5.82E+09	6.75E+09